Weakly Nonlinear Analysis for Hele-Shaw Problem: The Effect of Boundary Conditions

Hele-Shaw 問題に対する弱非線形解析: 境界条件の効果

Submitted to the Department of Physics,
Faculty of Science, Tokyo University of Science
As a thesis for the degree of Doctor of Science

Hisasi Tani (谷 文之)

Department of Physics
Faculty of Science
Tokyo University of Science

April 17, 2014

Abstract

We investigate the effect of two kinds of boundary conditions on the motion of an interface in Hele-Shaw cell, which is known as Hele-Shaw problem. The validity of Young–Laplace equation that was traditionally employed as a boundary condition for this problem, has been discussed, because the discrepancies in the motion of interface between theories and experiments exist. Then some corrections to the Young–Laplace equation have been introduced in order to obtain the more appropriate boundary condition. In the Thesis, we perform the weakly nonlinear analysis for Hele-Shaw problem using two kinds of boundary conditions.

First, we investigate the boundary conditions including the effect of viscous normal stress (VNS). Mode coupling equation is derived and weakly nonlinear analysis is carried out. The analytical results indicate that the effect of VNS enhances the instability of the interface. The approximated numerical solutions for the mode coupling equation are obtained from the analytical formulae. These results show that the nonlinear features of perturbed interfaces appeared more clearly than those in the previous studies. We thus conclude that the boundary condition with VNS clearly enhances the instability of the interface, and plays an important role for the nonlinear behaviours of the interface.

Second, we investigate the boundary condition including the effect of wetting layer of the displaced fluid in the Hele-Shaw cell. The mode coupling equation is derived for the boundary conditions in similar to the case of VNS. Then the weakly nonlinear analysis is carried out based on the boundary condition including the wetting effect. Considering the analytical and numerical results, we find that this boundary condition facilitates the instability more largely than the boundary condition with VNS effect. Nonlinear features of the unstable interface appear more clearly than those in the previous results by the Young–Laplace equation.

Thus we find that the corrections to the Young–Laplace equation enhance the instability of the interface in Hele-Shaw cell. Our results in the Thesis demonstrate the important role of the boundary conditions for the viscous fingering patterns.

Acknowledgements

The author would like to express his greatest appreciation to Professor Kazuyuki Watanabe of Department of Physics, Graduate School of Science, Tokyo University of Science, for his continuous advice and guidance. He would like to express his sincere appreciation to Assistant Professor Chunping Hu for giving fruitful advice and suggestions. Moreover, he would like to show his sincere gratitude to Assistant Professor Reiho Sakamoto and Associate Professor Takahiro Yajima for fruitful comments and discussions. He would also like to offer his special thanks to all the member of the research group under Professor Kazuyuki Watanabe, and theoretical group at the Tokyo University of Science, for fruitful discussions and suggestions.

Finally, the author would like to extend heartfelt appreciation to late Professor Miki Wadati for giving me the theme of the Thesis. He also wishes to express his deepest gratitude to Professor Tani and Mrs. Tani for their continuous guidance, discussions, and encouragement.

Contents

List of Figures

Chapter 1

Introduction

1.1 Pattern Formation in Nature

Nature is full of patterns: shape of a snow crystal, wind ripples on deserts, stripes of zebras and so on. We can see such patterns all over the world and have a question about mechanisms of their formation.

For example, historically, J. Kepler, who is famous for his laws about the progression of the planets, was interested in the reason why all snow crystals have hexagonal shapes in the early 17th century [1]. More recently, U. Nakaya studied their processes of growth systematically. He is well known as the first person to succeed in making artificial snow crystals. He revealed that shapes of snow crystals are determined by the condition of parameters of vapor, supersaturation, and temperature [2]. This was expressed as the Nakaya diagram (see, for instance, [3]). He is also famous for his words, 'snow is a letter from the sky'.

Such investigations about the patterns in nature are not only for the snow crystals. For instance, in the beginning of twentieth century, D. Thompson studied the form of animals, such as morphologies of fishes, from the mathematical point of view [4]. I. Prigogine and co-workers proposed that patterns or structures are organized in open systems far from equilibrium, known as dissipative systems [5]. A. Turing revealed that spatially inhomogeneous patterns are spontaneously formed under certain conditions for the diffusion coefficients of reaction-diffusion equations [6]. These researches are innovative and still investigated in a wide variety of fields of science. In fact, Belousov-Zhabotinsky reaction is one of the most well-known examples, whose spiral patterns are formed in a two-component chemical reaction-diffusion system [7, 8].

Formations of skin patterns of animals such as spots of panthers or stripes of zebras are widely studied as examples of patters due to Turing instability in the field of statistical physics, mathematics and computer science as well as biology. In 1995, Kondo and Asai suggested that skin patterns of a marine angelfish, *Pomacanthus* (Fig. 1.1), is determined by Turing instability [9].

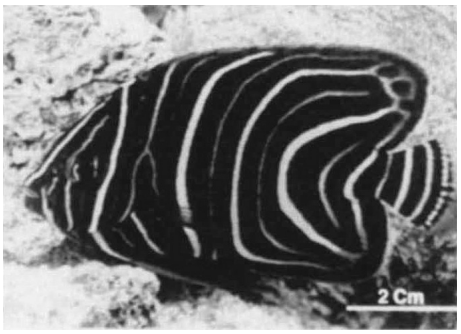

Figure 1.1: Skin patterns of a fish, due to Kondo and Asai [9]

Another example is the morphologies of bacteria colonies. It is well known that bacteria, *Bacillus subtilis*, form different types of their colonies from circular to fractal patterns like the ones by diffusion limited aggregation (DLA). These patterns are determined by their surroundings; the concentration of nutriment and the hardness of medium [10].

Among the investigations about the pattern formation, T. Terada was one of the first researchers who focus on the patterns in our daily life. He is famous as a researcher to study from geophysics to statistical physics, and also known as an essayist. In his essay [11] he remarked about the morphology of kompeito, formation of a crack of dry paste, and relationship between sparks of the sparkling fireworks and lightning. His simple and unique viewpoints about these phenomena give a wide variety of research topics even now.

Here, the meaning of the term 'pattern' should be clear. According to the Oxford Dictionary of English, 'pattern' means 'a regular and intelligible form or sequence discernible in the way in which something happens or is done'. This indicates that patterns exist where we recognize them; when we look at a shape of an interface or some repetitive structures in a system, we frequently guess there are some mechanisms beneath them, and eager to understand them. In general, it is known that pattern formations are caused by some instabilities. As mentioned above, Turing instability leads to the wavy patterns represented as Belousov-Zhabotinsky reaction. Rayleigh–Taylor instability, due to a difference between the densities of fluids, causes mushroom-like patterns. It is also well known that Kelvin–Helmholtz instability, due to a difference between the tangential velocities of fluids, causes triangle-wave patterns, which sometimes can be seen as forms of clouds . From these examples it can be mentioned in common that if the interfaces once become unstable, and perturbations develop rapidly, and finally some patterns are formed. Among these instabilities and patterns, one of the simplest and widely studied example is the Saffman–Taylor instability and viscous fingering phenomena

[12].

1.2 Hele-Shaw Problem

1.2.1 Viscous Fingering in the Rectangular Geometry

Saffman–Taylor instability, named after P. G. Saffman and G. I. Taylor, occurs due to a difference in viscosity between the fluids. They revealed that if the fluid with smaller viscosity displaces the one with larger viscosity then the interface becomes unstable and the growth of a lot of finger-like patterns appear as shown in Fig. 1.2. This phenomena is well known as 'viscous fingering'.

Experimental and theoretical studies on viscous fingering are classified into two groups: the rectangular geometries [12]-[17] explained below, and the radial ones [18]-[22] to be introduced in the next subsection.

In fact, Taylor [23] and Lewis [24] already showed the similar instability of an interface between two fluids with different densities. They pointed out that the interface becomes unstable if the less dense fluid displaces the more dense one, and fingering patterns are formed. After a while, Saffman and Taylor showed that such fingering phenomena occur due to the differences in viscosities of the fluids in a Hele-Shaw cell [12]. Here Hele-Shaw cell is an experimental instrument which consists of two parallel plates with a narrow gap so that one can observe two-dimensional hydrodynamical phenomena. It is named after H. S. Hele-Shaw, who was an engineer in the end of 19th century. He was interested in a method to visualize stream lines and invented a Hele-Shaw cell in 1897 after some trials and errors [25]. The Hele-Shaw cell is illustrated later in Fig. 2.2. Hele-Shaw carried out experimental studies by using the Hele-Shaw cell and reported that the flow is laminar at all velocities if the gap of the cell is sufficiently narrow [25]. Hele-Shaw cell has been used in a wide variety of fields of science such as hydrodynamics, soft matter physics,

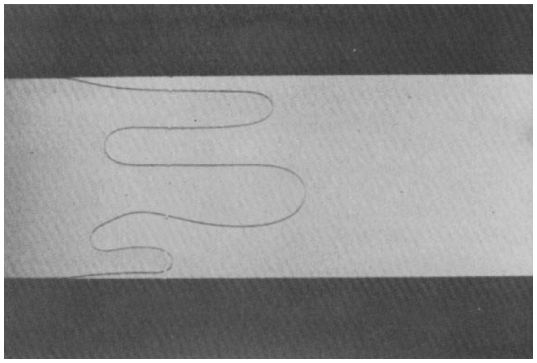

Figure 1.2: Fingering in a rectangular Hele-Shaw cell by Tabeling *et al.* [17]

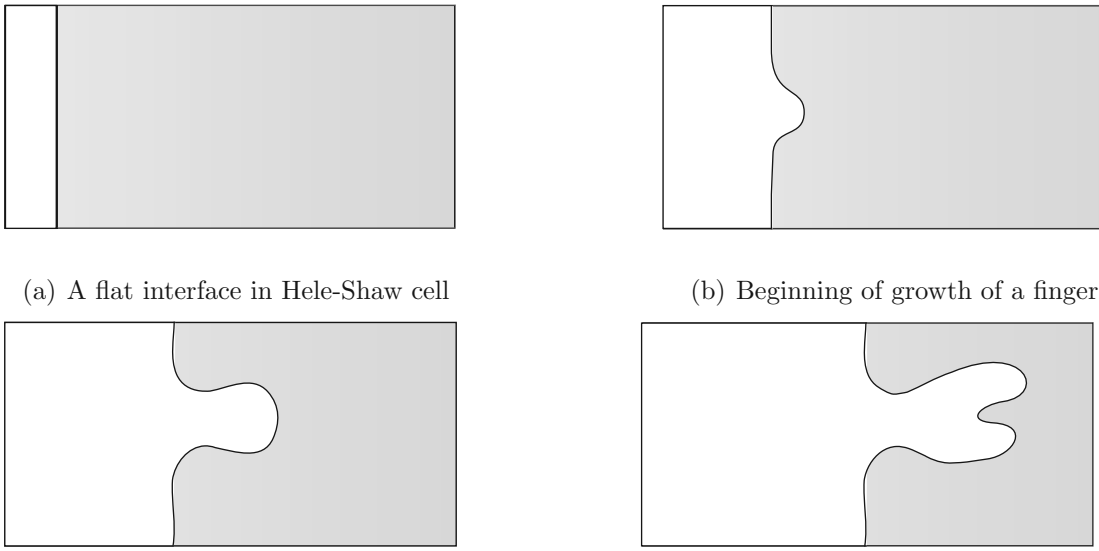

(a) A flat interface in Hele-Shaw cell

(b) Beginning of growth of a finger

(c) Tip-spreading of the finger

(d) Tip-splitting of the finger

Figure 1.3: The process of the fingering phenomena

and granular materials physics.

In the original experiment due to Saffman and Taylor [12], air is injected from one end of the rectilinear Hele-Shaw cell filled with glycerine, The air displaces the glycerine, and the interface is driven by the pressure and translating in the cell. This type of studies are referred to as the rectangular geometry. In this situation, it is known that an interface becomes unstable, and fingering patterns are formed by the following mechanism (Fig. 1.3). Let us consider a Hele-Shaw cell filled with viscous fluid. First the less viscous fluid is injected into the Hele-Shaw cell from the left, then an initially flat interface is driven to the right, as shown in Fig. 1.3(a). If the interface becomes locally convex, as depicted in Fig. 1.3(b), the pressure gradient at the tip is larger than the other part of the interface. This means that the convex part tends to be more convex to become a finger, which is similar to the Gibbs-Thomson effect for the crystal growth. Once fingers are formed then their tips become blunt and spreading as in Fig. 1.3(c), and finally the tips split (Fig. 1.3(d)), and the split fingers grow independently. It is known that tip-spreading and splitting appearing in these processes are features of viscous fingering phenomena [26]. In addition, Saffman and Taylor revealed that there exists a single stable finger translating in the cell with a constant velocity [12]. This is called Saffman–Taylor finger, and its behaviour is qualitatively understood by their analysis via the complex potential in [12].

1.2.2 Viscous Fingering in the Radial Geometry

So far we described the case that the less viscous fluid is injected from an end of the Hele-Shaw cell, as shown in Fig. 1.2, whose type is referred to as the rectangular geometry. On the other hand, in the case of the radial geometry, the less viscous fluid is injected from a point source on the cell plate (Fig. 1.4). As the less viscous fluid is injected, an initially circular interface becomes unstable and forms a radial fingering pattern. Figure 1.4 shows one of the typical experimental snapshots for the radial case [19]. Compared with the rectangular geometry, in the radial geometry it is an essential difference that there is no stable single-finger pattern like a Saffman–Taylor finger. Investigations in the radial geometry originally began as a model of injection into the underground soil [18], known as enhanced oil recovery in engineering [27, 28]. When we draw petroleum from underground, it is often necessary to keep oil pressure high in order to remain the flow from oil fields. For this purpose, water or some chemical solutions are usually injected into the oil field by using a pipe. This is the typical enhanced oil recovery method. Since the injection is from the end of the pipe and the injected fluids are spreading radially, it is more appropriate to consider in the radial geometry for this case.

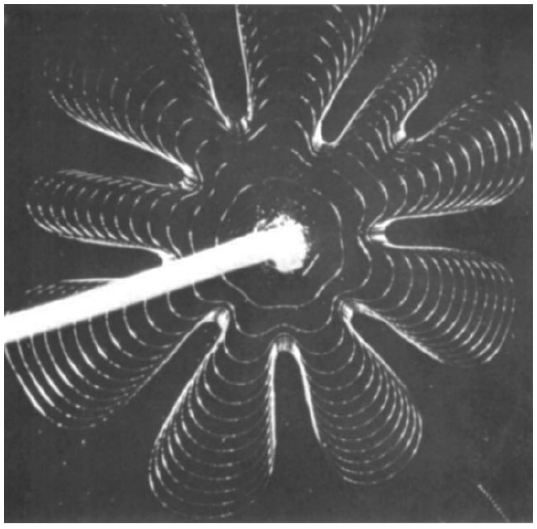

Figure 1.4: An example of the radial fingering, by Paterson [19]

In addition to these two groups, there are investigations about intermediate configurations. Thomé *et al.* investigated fingering patterns in the sector geometry [21]. In Fig. 1.4 one can observe some sector-like patterns formed by spreading fingers. It is worthwhile to investigate this type of geometry as a complement to the rectangular and radial ones.

1.2.3 Hele-Shaw Problem

In the previous subsections, we introduced viscous fingering phenomena in the Hele-Shaw cell. In this Thesis we focus on the viscous fingering in the case of radial geometry. However, it is to be noted that investigations about motions of interfaces in Hele-Shaw cells are not limited to

the fingering phenomena. For instance, the shape of a moving bubble in a horizontally placed Hele-Shaw cell is also investigated [29]. For the case of the perpendicular cell, this is known as the rising bubble problem [30, 31]. Another example is the finite source/sink model studied by P. Ya. Polubarinova-Kochina [32] and L. A. Galin [33]. The interface motion in radial geometry introduced in the previous subsection corresponds to the case of the source for this model. In their studies, Kochina [32] and Galin [33] used conformal mappings from the unit disk onto the fluid region, and independently derived equations about the time evolution of the interfaces, which is known as the Polubarinova-Galin equation [34]. The finite source/sink model is a simplified model of the oil industry [32], [33] and the moulding of molten polymer [35].

Thus, there are a variety of problems related with the motions of interfaces in Hele-Shaw cells. In general, such problems, concerned with an interface motion in the Hele-Shaw cell, are referred to as Hele-Shaw problems. Hele-Shaw problem is often studied as a one-phase free boundary problem by regarding the less viscous fluid as the inviscid one. On the other hand, two-phases Hele-Shaw problem is sometimes referred to as Muskat problem. In the Thesis, we simply refer these two problems as the Hele-Shaw problem, and study only the case of two-phases.

1.2.4 Radial Fingering Patterns and Related Phenomena

As mentioned above, an interface motion in the Hele-Shaw cell is associated with some applications such as oil recovery or moulding. In this subsection, we introduce the other examples which are often related with the radial fingering. First example is the growth of a dendrite crystal. In general, anisotropy originating from the molecular structure of the crystal plays an important role on the morphology of the crystal. In the case of viscous fingering, it is known that if an anisotropy of growth velocity is introduced, then fingering patterns change into the dendrite shapes. In many cases, such anisotropy is produced by trenches, which are engraved in the Hele-Shaw cell. Along with the trenches, fingers grow more rapidly and the shape of the interface is no more circular. Under such a situation, it is observed that side branches are produced from the finger as in Fig. 1.5. Therefore, Hele-Shaw problem is often studied in relation to the morphologies of snow crystals [36]-[38]. Actually, it is not only matter of the appearances; their mechanisms are closely related to each other. As will be seen in Chapter 3, Hele-Shaw problem results in solving the Laplace equation for the velocity potential under two boundary conditions. On the other hand, crystal growth obeys the heat diffusion equation, which is

equivalent to the Laplace equation for the stationary case, under the similar types of boundary conditions. Thus, viscous fingering is close to the dendrite patterns of the crystal growth.

Another example is the patterns formed by bacterial colonies mentioned in Introduction, which resembles closely to the radial fingering patterns [10]. As mentioned above, bacteria known as *Bacillus subtilis* form their colonies with patterns as shown in Figs. 1.6 and 1.7 [39]. It is interesting to note that these patterns seem to be quite similar to the viscous fingering patterns in a Hele-Shaw cell in Fig. 1.4. Moreover, though it is beyond the scope of the Thesis, this problem was also studied as the motion of curves in the context of the integrable hierarchy [40], and was associated with string theory [34, 41], or quantum Hall regime [42]. Thus, Hele-Shaw problems are old and new problems to be studied further. In spite of its quite simple formulation, the Hele-Shaw problem certainly covers a wide variety of phenomena (for more examples, see [43]). This is the reason why Hele-Shaw problems have been intensively studied both in the theoretical and the experimental fields of physics.

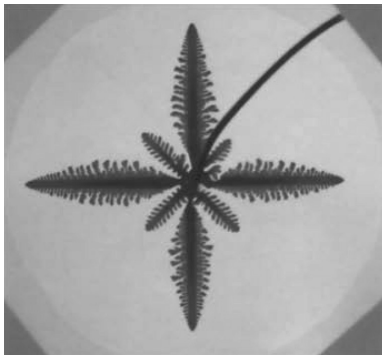

Figure 1.5: Viscous fingering with anisotropy, by Chen [38]

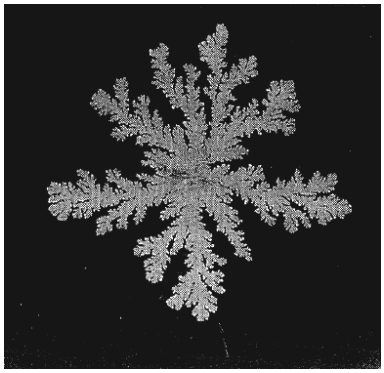

Figure 1.6: Fractal patterns of bacterial colonies, by Ohgiwari *et al.* [39]

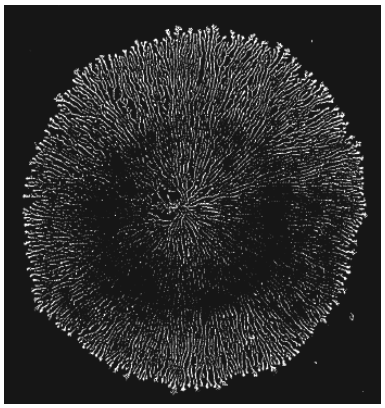

Figure 1.7: Circular patterns of bacterial colonies, by Ohgiwari *et al.* [39]

1.2.5 Contents of the Thesis

Motivated by the universal properties of the Hele-Shaw problem mentioned above, we investigate the morphologies of radial fingering patterns in the Hele-Shaw theoretically. The contents of the Thesis are as follows.

In Chapter 2, we briefly review the fundamental formulations of mathematical fluid dynamics. There, we begin with the conservation laws, and derive the basic equations for fluid dynamics and constitutive equations for incompressible Newtonian fluids. Then Hele-Shaw equation, which is a governing equation for flows in the Hele-Shaw cell, is derived.

In Chapter 3, a theoretical approach to Hele-Shaw problem is introduced. First, it is indicated that the Hele-Shaw problem leads to the Laplace equations for velocity potentials of fluids. Second, the boundary conditions for Laplace equations are introduced, and their validities are discussed. Finally, we explain the mode coupling equation proposed in the previous studies. This equation was derived and often used by Miranda and co-author [44].

In Chapter 4, we describe one of our original results. Some problems about boundary conditions that have been studied so far are pointed out and discussed. We employ the new boundary condition including the effect of viscous normal stress terms, and derive the extended mode coupling equation. Numerical solutions obtained by integrating the extended mode coupling equation support the validity of our model.

The other kind of boundary condition is investigated in Chapter 5. We obtain our results from the present boundary condition, which is derived from the wetting phenomena of Hele-Shaw cells. Both analytical and numerical results are shown, and the relationship between the models in Chapters 4 and 5 is discussed.

Finally, conclusion in the Thesis is given in Chapter 6.

Chapter 2

Governing Equations for Hele-Shaw Flow

In this chapter, we begin with the fundamental formulation of fluid dynamics, and then proceed to the derivation of governing equations for flows in a Hele-Shaw cell. First the definition of fluid and two methods to describe the fluid, Lagrangian and Eulerian descriptions, are introduced. Then we see that the conservation laws with the convection theorem lead the fundamental equations of fluid dynamics. Second, the constitutive equations for the incompressible Newtonian fluid is considered. Finally, the governing equations for Hele-Shaw flow are derived from these equations.

2.1 Fundamentals in Fluid Dynamics

First of all, let us give the definition of the fluid; it is used in common as a material which has flowing behaviour, *i.e.*, deforms easily to external forces, such as liquid and gas. Assume that a macroscopic feature of a system varies with the scale L, and the mean free path of molecules consisting of the system is l. If $L \gg l$ holds, then the system can be regarded as the homogeneous material which has a continuously-distributed mass. This is the continuum hypothesis [45], and material which satisfies this hypothesis is referred to as the continuum. Continuum is roughly classified into three groups: elastic, plastic, and fluid. Usually, both elastic and plastic materials are referred to as 'solid', which deform 'a little' by external forces. On the other hand, 'fluid' deforms 'largely' under such an external force, and is distinguished from 'solid'

thereby. However, it should be noted that such a classification is rather naive because a lot of fluids around us also show the elastic or plastic features. For instance, mayonnaise behaves as a plastic under a small stress; it does not happen, as everybody knows, that mayonnaise diffuses spontaneously and wet all over the dish. On the contrary, if a large stress is added to squeeze the tube, then mayonnaise shows fluidity. This is an example of the Bingham plastic, named after E. C. Bingham who proposed its mathematical formulation [46]. Another example is a mixture of cornstarch and water, known as a dilatant (or a shear-thickening) material. A dilatant material behaves as a fluid at a small stress, while behaves like a rigid body with a large stress [47]. Because of this property, we can walk on the surface of a pool filled with cornstarch-water mixture without sinking down, as long as we step the surface strongly enough. These examples tell us that it is not so easy to define if a continuum is simply a 'fluid' or a 'solid': what we can say seems that the continuum exhibits fluid-like or solid-like behaviour under some conditions. Compared with the examples above, the water and the air behave more simply. They deform by infinitesimal external forces: more correctly, their rate of deformations are proportional to the shear stresses. Such fluids are known as Newtonian fluids, which are introduced in the following subsection. These relationships between the shear stresses and the rate of deformations determine the characteristic features of the fluids. For the Newtonian fluid, the relationship is linear. While for the Bingham plastics or dilatant fluids, the relationships are nonlinear, which cause their complicated behaviours as shown in the above examples. In addition, an ideal fluid is defined as an imaginary material which has no resistance to shear stresses.

2.1.1 Lagrangian and Eulerian Description

In order to describe a motion of a fluid, what we have to know is the velocity vector $\boldsymbol{v} = (v_1, v_2, v_3)$ of the flow. These three components of $\boldsymbol{v}$ are determined by solving the conservation laws of mass, momentum, and energy, as shown in the following subsections. In addition to the velocity vectors, thermodynamical states of the fluid have to be determined by two thermodynamical variables, typically the pressure P and the density ρ, out of five. Thus we should deal with these five unknown hydrodynamical quantities: three components of velocity vector and two thermodynamical variables. Now the flow can be completely determined in principle since we have five equations for five unknown variables: conservation equations for mass, energy, and three components of momentum.

There are two well-known methods to describe the velocity vector of the flow: Lagrangian

and Eulerian descriptions (for instance, [45]). Lagrangian description is to investigate how the hydrodynamical quantities of a fluid particle are varying with the flow. This method is, in other words, to observe motions of a marker on the fluid and know about the flow thereby. Here, we should notice that the term 'fluid particle' represents a small fragment of the fluid within the regime where the continuum hypothesis holds. In a Lagrangian description, the independent variable of the velocity vector $\boldsymbol{v}$ is time t and each fluid particle is identified by the continuous label $\boldsymbol{a}$. One simple example of $\boldsymbol{a}$ is the position vector at $t = 0$. Then the velocity can be represented as .

$$\boldsymbol{v} = (v_1(\boldsymbol{a}, t), v_2(\boldsymbol{a}, t), v_3(\boldsymbol{a}, t)) .$$

Lagrangian description is convenient in some special cases, however, usually it is inconvenient since the spatial variance of the flow is not obtained directly. In many cases, we are more interested in how the flow is at each point of the field. This is an Eulerian description, that investigates how the hydrodynamical quantities at any point vary with time. This method is, that is to say, to observe the physical quantities of the flow on a buoy floating at any point. In general, Eulerian description is used because each particle of fluid is essentially the same in the most cases, and therefore it is more convenient to understand the flow by the field rather than the particles. In Eulerian description, the independent variables are position $\boldsymbol{x}$ of the field and time t. Then the velocity can be represented as

$$\boldsymbol{v} = (v_1(\boldsymbol{x}, t), v_2(\boldsymbol{x}, t), v_3(\boldsymbol{x}, t)) .$$

Following is the important transformation between the Lagrangian and the Eulerian descriptions:

$$\frac{\mathrm{D}}{\mathrm{D}t} = \frac{\partial}{\partial t} + \boldsymbol{v} \cdot \nabla, \tag{2.1.1}$$

which is known as the material (or substantial) time derivative.

Here, in order to define the motions of fluid mathematically, we consider a domain consisted of the same fluid particles. Let Ω_0 and Ω_t be domains in E^3 at $t = 0$ and t, respectively. It is assumed that fluid particles which is included in an initial domain Ω_0 is translating and remains to be included Ω_t at time t. Then 'fluid motion' is equivalent to hold

$$\Omega_t = H_t \, \Omega_0. \tag{2.1.2}$$

Here H_t is a smooth transformation on the closure $\overline{\Omega_0}$. The schematic picture of this relationship (2.1.2) is as depicted in Fig. 2.1. By using the transformation H_t, the motion of free surface $\mathscr{F}$

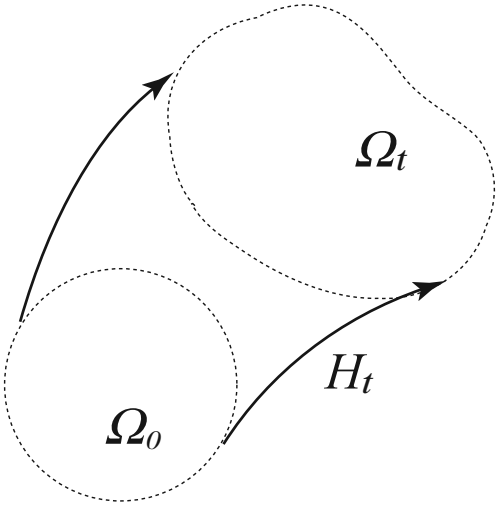

Figure 2.1: The motion of fluid

is also expressed as

$$\mathscr{F}(t) = H_t\,\mathscr{F}(0). \tag{2.1.3}$$

Here $\mathscr{F}(0)$ and $\mathscr{F}(t)$ denote the surface at $t = 0$ and t, respectively [48].

2.1.2 Convection Theorem

One of the most fundamental theorems in fluid dynamics is the following one [48]:

Convection Theorem

If Ω_t is a fluid domain, and if $f(\boldsymbol{x}, t) \in C^1(\overline{\Omega_t})$, then

$$\frac{\mathrm{d}}{\mathrm{d}t}\int_{\Omega_t} f\,\mathrm{d}V = \int_{\Omega_t}\left(\frac{\mathrm{D}f}{\mathrm{D}t} + f\,\nabla\cdot\boldsymbol{v}\right)\mathrm{d}V, \tag{2.1.4}$$

where $\mathrm{d}V$ denotes the volume element.

From this theorem, the following corollary implies.

Corollary 2.1.1

With Ω_t and f as in the convection theorem, let Ω_1 be the fixed domain in E^3 which coincides with Ω_t at $t = t_1$ and has a regular surface $\partial\Omega_1$. Then at an arbitrary time t_1

$$\frac{\mathrm{d}}{\mathrm{d}t}\int_{\Omega_t} f\,\mathrm{d}V\bigg|_{t=t_1} = \frac{\partial}{\partial t}\int_{\Omega_1} f\,\mathrm{d}V + \int_{\partial\Omega_1} f\,\boldsymbol{v}\cdot\mathbf{n}\,\mathrm{d}S, \tag{2.1.5}$$

where $\mathbf{n}$ is the unit outward normal, and $\mathrm{d}S$ the surface element on $\partial\Omega_1$.

A proof is given in Appendix. By using Eqs. (2.1.4) and (2.1.5) to the conservation equations introduced in the following subsections, fundamental equations will be derived such as the continuity equation and the equation of motion.

2.1.3 Mass Conservation

This postulate represents that mass of fluid initially included in a domain is conserved, neither increasing nor decreasing spontaneously. Let $\rho(\boldsymbol{x}, t)$ be defined on the closure of any fluid domain $\Omega_t = H_t\Omega_0$ so that for all t

$$\int_{\Omega_t} \rho \, \mathrm{d}V = m(\Omega_0) > 0, \tag{2.1.6}$$

where m denotes the mass of the fluid which is determined by the initial domain Ω_0, and ρ represents its density. From Eqs. (2.1.4) and (2.1.6), it follows

$$\begin{aligned} \frac{\mathrm{d}}{\mathrm{d}t}\int_{\Omega_t} \rho \, \mathrm{d}V &= \int_{\Omega_t} \left(\frac{\mathrm{D}\rho}{\mathrm{D}t} + \rho \nabla \cdot \boldsymbol{v} \right) \mathrm{d}V \\ &= 0. \end{aligned} \tag{2.1.7}$$

Similarly, Eq. (2.1.5) to Eq. (2.1.6) yields

$$\begin{aligned} \frac{\mathrm{d}}{\mathrm{d}t}\int_{\Omega_t} \rho \, \mathrm{d}V \bigg|_{t=t_1} &= \frac{\partial}{\partial t}\int_{\Omega_1} \rho \, \mathrm{d}V + \int_{\partial\Omega_1} \rho \, \boldsymbol{v} \cdot \mathbf{n} \, \mathrm{d}S \\ &= \int_{\Omega_1} \left(\frac{\partial \rho}{\partial t} + \nabla \cdot (\rho \boldsymbol{v}) \right) \mathrm{d}V \\ &= 0. \end{aligned} \tag{2.1.8}$$

Here we uses the Gauss' divergence theorem

$$\int_{\partial\Omega_1} \boldsymbol{v} \cdot \mathbf{n} \, \mathrm{d}S = \int_{\partial\Omega_1} \nabla \cdot \boldsymbol{v} \, \mathrm{d}V. \tag{2.1.9}$$

Eqs. (2.1.7) and (2.1.8) give the following relations.

$$\frac{\mathrm{D}\rho}{\mathrm{D}t} + \rho \nabla \cdot \boldsymbol{v} = 0, \tag{2.1.10}$$

$$\frac{\partial \rho}{\partial t} + \nabla \cdot (\rho \boldsymbol{v}) = 0. \tag{2.1.11}$$

These equations (2.1.10) and (2.1.11) are known as the continuity equation in the Lagrange and the Eulerian descriptions, respectively. In some cases, ρ can be regarded as an invariant

with respect to the motion of the fluid, which is

$$\frac{\mathrm{D}\rho}{\mathrm{D}t} = 0. \tag{2.1.12}$$

Fluids obeying Eq. (2.1.12) are referred to as incompressible. Thus the continuity equation for the incompressible fluids can be written simply as

$$\nabla \cdot \boldsymbol{v} = 0. \tag{2.1.13}$$

It should be noted that a fluid with $\rho = const.$ is incompressible, however, the converse does not always hold; even though $\rho(\boldsymbol{x}, t)$ varies in Eulerian description, it is referred to as an incompressible fluid as far as it satisfies $\mathrm{D}\rho/\mathrm{D}t = 0$. A fluid can be considered as incompressible, if its velocity $\boldsymbol{v}$ is small enough compared to the sound speed.

2.1.4 Momentum Conservation

Conservation laws of the linear and the angular momentum are also the most fundamental and as important as the conservation law of mass. From the linear momentum theorem, which is essentially identical to the Newton's second law, the equation of motion for fluids is derived. On the other hand, from the angular momentum theorem, the symmetry of stress tensor is derived. For an arbitrary system with material flow through it, Newton's second law states that the rate of change of the linear momentum is equal to the sum of the external forces acting on a system

$$\frac{\mathrm{d}}{\mathrm{d}t}\int_{\Omega_t} \rho\,\boldsymbol{v}\,\mathrm{d}V = \int_{\Omega_t} \rho\boldsymbol{f}\,\mathrm{d}V + \int_{\partial\Omega_t} \boldsymbol{T}^{(n)}\,\mathrm{d}S, \tag{2.1.14}$$

where $\boldsymbol{T}^{(n)} = \mathbf{n}\cdot\mathbf{T}$ is the normal stress vector, and $\mathbf{n}$ is the unit outward normal to $\partial\Omega_t$. Here $\mathbf{T}$ is the stress tensor of the fluid. The left hand side of Eq. (2.1.14) represents the rate of change of the linear momentum, and the first and second terms in the right hand side express the body force $\rho\boldsymbol{f}$ acting on each volume element of the fluid and the normal stress $\boldsymbol{T}^{(n)}$ acting on the surface of the fluid, respectively. Due to the Gauss' divergence theorem, Eq. (2.1.14) becomes,

$$\frac{\mathrm{d}}{\mathrm{d}t}\int_{\Omega_t} \rho\,\boldsymbol{v}\,\mathrm{d}V = \int_{\Omega_t} \rho\boldsymbol{f}\,\mathrm{d}V + \int_{\partial\Omega_t} \nabla\cdot\mathbf{T}\,\mathrm{d}V \tag{2.1.15}$$

By using Eqs. (2.1.4) and (2.1.10), the left hand side of Eq. (2.1.15) can be transformed as

$$\begin{aligned}\frac{\mathrm{d}}{\mathrm{d}t}\int_{\Omega_t}\rho\,\boldsymbol{v}\,\mathrm{d}V &= \int_{\Omega_t}\left(\frac{\mathrm{D}(\rho\,\boldsymbol{v})}{\mathrm{D}t}+\rho\,\boldsymbol{v}\,\nabla\cdot\boldsymbol{v}\right)\mathrm{d}V\\ &= \int_{\Omega_t}\left(\frac{\mathrm{D}\rho}{\mathrm{D}t}\,\boldsymbol{v}+\rho\,\frac{\mathrm{D}\boldsymbol{v}}{\mathrm{D}t}+\rho\,\boldsymbol{v}\,\nabla\cdot\boldsymbol{v}\right)\mathrm{d}V\\ &= \int_{\Omega_t}\rho\,\frac{\mathrm{D}\boldsymbol{v}}{\mathrm{D}t}\,\mathrm{d}V. \end{aligned} \tag{2.1.16}$$

Therefore, Eqs. (2.1.15) and (2.1.16) imply

$$\int_{\Omega_t}\rho\,\frac{\mathrm{D}\boldsymbol{v}}{\mathrm{D}t}\,\mathrm{d}V=\int_{\Omega_t}\rho\boldsymbol{f}\,\mathrm{d}V+\int_{\partial\Omega_t}\nabla\cdot\mathbf{T}\,\mathrm{d}V \tag{2.1.17}$$

for any domain Ω_t, and then the equation of motion is derived as

$$\rho\,\frac{\mathrm{D}\boldsymbol{v}}{\mathrm{D}t}=\nabla\cdot\mathbf{T}+\rho\boldsymbol{f}. \tag{2.1.18}$$

Equation (2.1.18) is also known as Cauchy's momentum equation.

Similarly to the linear momentum in the above, we consider a conservation law of the angular momentum. It is written as

$$\frac{\mathrm{d}}{\mathrm{d}t}\int_{\Omega_t}\rho\,\boldsymbol{x}\times\boldsymbol{v}\,\mathrm{d}V=\int_{\Omega_t}\boldsymbol{x}\times\rho\boldsymbol{f}\,\mathrm{d}V+\int_{\partial\Omega_t}\boldsymbol{x}\times\boldsymbol{T}^{(n)}\,\mathrm{d}S. \tag{2.1.19}$$

This conservation equation (2.1.19) leads to the symmetry of the stress tensor

$$T_{ij}=T_{ji},\quad (i,j=1,2,3) \tag{2.1.20}$$

where T_{ij} is (i,j)-component of the stress tensor (for the proof, see [48]).

It should be emphasized that conservation laws for mass (Eq. (2.1.6)), linear momentum (2.1.14), and angular momentum (Eq. (2.1.19)) hold for all continuum. However, symmetry of the stress tensor does not always hold; for instance, flow in some polarized media whose field couples with the body of fluid.

2.1.5 Constitutive Equation for Newtonian Fluids

Conservation laws in the previous subsection are the most fundamental since they hold for any kinds of fluids. However, these laws do not give us any information about the characteristic features of fluids such as water, mayonnaise, and cornstarch-water mixture, as mentioned in the beginning of this section. The differences between the feature of such a fluid are caused by the

relationship between stress and rate of deformation. Here, we consider the most fundamental case that the rate of deformation is proportional to the stress, known as the Newton's law. Such fluids, for instance water, air, and oil, are referred to as Newtonian fluids. In this subsection, constitutive equation for Newtonian fluid is derived.

In general, the stress can be related with the hydrostatic pressure for a fluid at rest as

$$\mathbf{T} = -\bar{p}\,\mathbf{I}, \tag{2.1.21}$$

where $\mathbf{I}$ is an identity tensor, and $\bar{p} = \bar{p}(\boldsymbol{x}, t)$ is defined by the isotropy of the stress in fluid at rest as

$$\bar{p} = \frac{1}{3}\operatorname{tr}\mathbf{T}, \tag{2.1.22}$$

which is referred to as the hydrostatic pressure of the fluid. Here, it should be noted that the hydrostatic pressure $\bar{p}$ is defined from a kinetic point of view, and therefore it is not always equal to the thermodynamical pressure p [48, 49]. For the case of an ideal fluid, it is known that $\bar{p}$ is identical to p, and its constitutive equation is

$$\mathbf{T} = -p\,\mathbf{I}. \tag{2.1.23}$$

Then, because of the Galilean relativity, it is expected that the equation (2.1.23) also holds for unidirectionally uniform flow, such that the velocity $\boldsymbol{v}$ of fluid in a domain Ω_t is constant. This equation (2.1.23) can be extended for a general flow, as

$$\mathbf{T} = -p\,\mathbf{I} + \boldsymbol{\tau}, \tag{2.1.24}$$

where $\boldsymbol{\tau}$ represents the deviation from a unidirectional flow. As indicated below, $\boldsymbol{\tau}$ shall be referred to as the viscous stress tensor if $\bar{p}$ is related to the thermodynamical pressure p.

Now we see that the effect of the body forces $\boldsymbol{f}$ can be included into pressure. Since the linear momentum conservation (2.1.14) for unidirectional flow yields

$$\begin{aligned}
\frac{\mathrm{d}}{\mathrm{d}t}\int_{\Omega_t}\rho\,\boldsymbol{v}\,\mathrm{d}V &= \int_{\Omega_t}\rho\,\frac{\mathrm{D}\boldsymbol{v}}{\mathrm{D}t}\,\mathrm{d}V \\
&= \int_{\Omega_t}\rho\boldsymbol{f}\,\mathrm{d}V + \int_{\partial\Omega_t}\mathbf{n}\cdot\mathbf{T}\,\mathrm{d}S \\
&= \int_{\Omega_t}\rho\boldsymbol{f}\,\mathrm{d}V - \int_{\partial\Omega_t}p\,\mathbf{n}\,\mathrm{d}S \\
&= 0
\end{aligned} \tag{2.1.25}$$

by substituting the constitutive equation (2.1.21) for unidirectional flow, and $\mathrm{D}\boldsymbol{v}/\mathrm{D}t = 0$ for the uniform flow. Therefore, because of the Gauss' divergence theorem,

$$\begin{aligned}\int_{\Omega_t} \rho \boldsymbol{f}\, \mathrm{d}V &= \int_{\partial\Omega_t} p\, \mathbf{n}\, \mathrm{d}S \\ &= \int_{\Omega_t} \nabla p\, \mathrm{d}V. \end{aligned} \tag{2.1.26}$$

As a result we can obtain the following hydrostatic law [45, 48]:

$$\rho \boldsymbol{f} = \nabla p. \tag{2.1.27}$$

This law (2.1.27) determines the hydrostatic pressure for the case of uniform, unidirectional flow.

For the class of the external force with a potential Φ, $\boldsymbol{f} = -\nabla\Phi$, if the motion is incompressible or ρ depends only on Φ, then the external force need not be explicitly considered by defining $\tilde{p}$ in place of $\bar{p}$

$$\tilde{p} = p - \int^{\boldsymbol{x}} \rho \nabla \Phi \cdot \mathrm{d}\boldsymbol{x}. \tag{2.1.28}$$

In fact, substituting Eqs. (2.1.24) and (2.1.28) into the momentum conservation (2.1.14), we have

$$\begin{aligned}\frac{\mathrm{d}}{\mathrm{d}t}\int_{\Omega_t} \rho \boldsymbol{v}\, \mathrm{d}V &= \int_{\Omega_t} \rho \boldsymbol{f}\, \mathrm{d}V + \int_{\partial\Omega_t} \mathbf{n}\cdot\mathbf{T}\, \mathrm{d}S \\ &= \int_{\Omega_t} \rho \boldsymbol{f}\, \mathrm{d}V + \int_{\partial\Omega_t} (-p\,\mathbf{I} + \boldsymbol{\tau})\cdot\mathbf{n}\, \mathrm{d}S \\ &= \int_{\Omega_t} \rho \boldsymbol{f}\, \mathrm{d}V - \int_{\partial\Omega_t} \left(\tilde{p}\,\mathbf{I} + \int^{\boldsymbol{x}} \rho \nabla\Phi\cdot\mathrm{d}\boldsymbol{x} + \boldsymbol{\tau}\right)\cdot\mathbf{n}\, \mathrm{d}S \\ &= \int_{\partial\Omega_t} (-\tilde{p}\,\mathbf{I} + \boldsymbol{\tau})\cdot\mathbf{n}\, \mathrm{d}S. \end{aligned} \tag{2.1.29}$$

Therefore, it is more convenient to use $\tilde{p}$ defined by

$$\begin{aligned}\tilde{p} &= p - \int^{\boldsymbol{x}} \rho \nabla\Phi\cdot\mathrm{d}\boldsymbol{x} \\ &= -\frac{1}{3}\operatorname{tr}\mathbf{T} - \int^{\boldsymbol{x}} \rho \nabla\Phi\cdot\mathrm{d}\boldsymbol{x} \end{aligned} \tag{2.1.30}$$

instead of p, which is referred to as the mean hydrodynamic pressure. Usually, in fluid dynamics, the word 'pressure' indicates the mean hydrodynamic pressure (2.1.30) [48]. Therefore, in this Thesis 'pressure', denoted by p as customary, represents the mean hydrodynamic pressure $\tilde{p}$.

The general form of the constitutive equation is

$$\mathbf{T} = -p\,\mathbf{I} + \boldsymbol{\tau}(\mathbf{e}), \tag{2.1.31}$$

where $\boldsymbol{\tau}(\mathbf{e})$ is a tensor function of the rate of strain tensor $\mathbf{e}$, whose component is defined as

$$\mathrm{e}_{ij} = \frac{1}{2}\left(\frac{\partial v_i}{\partial x_j} + \frac{\partial v_j}{\partial x_i}\right). \quad (i,j = 1,2,3) \tag{2.1.32}$$

As mentioned above, the characteristic features of fluids are determined by the functional form of $\boldsymbol{\tau}$. Especially, if $\boldsymbol{\tau}$ is linear with respect to $\mathbf{e}$, known as the Newton's law, then the fluid is referred to as the Newtonian fluid. Air, water and oil are examples of the Newtonian fluid. On the other hand, coal tar, mayonnaise, and polymer solution are categorized as the non-Newtonian fluid. Thus, the Newtonian fluid is characterized by the explicit representation of $\boldsymbol{\tau}$

$$\boldsymbol{\tau} = \lambda(\mathrm{tr}\,\mathbf{e})\,\mathbf{I} + 2\mu\mathbf{e}, \tag{2.1.33}$$

which is known as the Navier–Poisson's law [49]. Here, μ and λ denote the shear viscosity and the second viscosity, respectively.

Next, we see the condition that pressure $\bar{p}$, introduced from a kinematic point of view, is equivalent to the thermodynamical pressure p,. Let the components of the deviatoric stress be

$$\begin{aligned} \tau'_{ij} &= \mathrm{T}_{ij} - \frac{1}{3}\,\mathrm{T}_{kk}\delta_{ij} \\ &= \mathrm{T}_{ij} + \bar{p}\,\delta_{ij}, \end{aligned} \tag{2.1.34}$$

and the deviatoric rate of strain tensor be

$$\mathrm{e}'_{ij} = \mathrm{e}_{ij} - \frac{1}{3}\,\mathrm{e}_{kk}\delta_{ij}. \tag{2.1.35}$$

Since T_{ij} is given by Eq. (2.1.31), it follows

$$\begin{aligned} \tau'_{ij} &= (\bar{p} - p)\delta_{ij} + \lambda\,\mathrm{e}_{kk}\delta_{ij} + 2\mu\mathrm{e}_{ij} \\ &= (\bar{p} - p)\delta_{ij} + \left(\lambda + \frac{2}{3}\mu\right)\mathrm{e}_{kk}\delta_{ij} + 2\mu\mathrm{e}'_{ij}. \end{aligned} \tag{2.1.36}$$

Because of their definition, diagonal components of $\boldsymbol{\tau}'$ and $\mathbf{e}'$ are zero, and therefore for the case that $i = j$ in Eq. (2.1.36)

$$(\bar{p} - p) + \kappa\,\mathrm{tr}\,\mathbf{e} = 0. \tag{2.1.37}$$

Here the coefficient κ is defined as

$$\kappa = \lambda + \frac{2}{3}\mu, \tag{2.1.38}$$

which is known as the bulk viscosity. Therefore, the relationship between $\bar{p}$ and p is

$$\bar{p} = p - \kappa \operatorname{tr} \mathbf{e}. \tag{2.1.39}$$

As a result, the condition that $\bar{p}$ is identical to p is either $\kappa = 0$ or $\operatorname{tr} \mathbf{e} = 0$. The former condition, $\kappa = 0$, is known as the Stokes' hypothesis which is not always satisfied due to [50]. On the other hand, the latter means the fluid is incompressible since $\operatorname{tr} \mathbf{e} = \operatorname{div} \boldsymbol{v}$ [51]. Hence, for the incompressible fluids

$$\bar{p} = p \tag{2.1.40}$$

holds. In such a case, τ'_{ij} becomes

$$\begin{aligned} \tau'_{ij} &= 2\mu \mathrm{e}'_{ij} \\ &= 2\mu \mathrm{e}_{ij} - \frac{1}{3} \mathrm{e}_{kk} \delta_{ij} \\ &= 2\mu \mathrm{e}_{ij}. \end{aligned} \tag{2.1.41}$$

Finally, the constitutive equation for an incompressible Newtonian fluid is

$$\mathbf{T} = -p\,\mathbf{I} + 2\mu \mathbf{e}. \tag{2.1.42}$$

2.1.6 Navier-Stokes Equations

By substituting the constitutive equation (2.1.42) into the equation of motion (2.1.18), the governing equation for the incompressible Newtonian fluid is derived as follows:

$$\begin{aligned} \rho \frac{\mathrm{D}\boldsymbol{v}}{\mathrm{D}t} &= \rho \boldsymbol{f} + \nabla \cdot \mathbf{T} \\ &= \rho \boldsymbol{f} - \nabla p + 2\mu \nabla \cdot \mathbf{e}, \end{aligned} \tag{2.1.43}$$

which is known as the Navier-Stokes equations. When we consider the case of no external force, Eq. (2.1.43) is written as

$$\rho \frac{\mathrm{D}\boldsymbol{v}}{\mathrm{D}t} = -\nabla p + \mu \nabla^2 \boldsymbol{v}. \tag{2.1.44}$$

It should be emphasized that the Navier-Stokes equations (2.1.44) are obtained by using the constitutive equation (2.1.42), so that they only hold for Newtonian fluids. In this Thesis, we deal with the incompressible Newtonian fluid, and investigate the motion of an interface between two Newtonian fluids.

2.2 Hele-Shaw Equation

2.2.1 Derivation of Hele-Shaw Equation

In this subsection, we derive a governing equation for flows in the Hele-Shaw cell, which is found in the famous text of hydrodynamics by Lamb [52]. The governing equation, hereafter called Hele-Shaw equation, can be derived from the incompressible Navier-Stokes equations without external forces (2.1.44). Take the x_1-, x_2-, and x_3-axis as shown in Fig. 2.2, and let the velocity of flow be $\boldsymbol{v} = (v_1, v_2, v_3)$ where v_i is the x_i component of the flow ($i = 1, 2, 3$). Then the

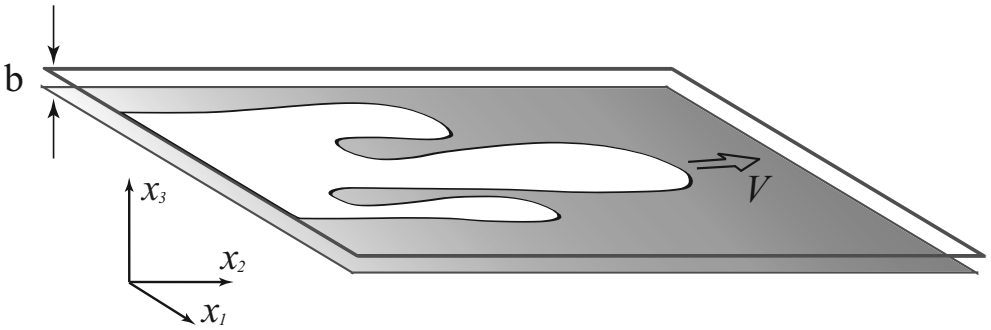

Figure 2.2: The schematic picture of a flow in the Hele-Shaw cell

incompressible Navier-Stokes equations are

$$\frac{\partial \boldsymbol{v}}{\partial t} + (\boldsymbol{v} \cdot \nabla)\boldsymbol{v} = \frac{1}{\rho}\left(-\nabla p + \mu \nabla^2 \boldsymbol{v}\right), \tag{2.2.1}$$

$$\nabla \cdot \boldsymbol{v} = 0. \tag{2.1.13}$$

We assume that the flow is steady and parallel to the x_1x_2-plane:

$$\frac{\partial v_1}{\partial t} = \frac{\partial v_2}{\partial t} = 0, \tag{2.2.2}$$

$$v_3 = 0. \tag{2.2.3}$$

With these assumptions the Navier-Stokes equations (2.2.1), (2.1.13) lead to

$$\left(v_1 \frac{\partial}{\partial x_1} + v_2 \frac{\partial}{\partial x_2}\right) v_1 = -\frac{1}{\rho}\frac{\partial p}{\partial x_1} + \frac{\mu}{\rho}\nabla^2 v_1, \tag{2.2.4}$$

$$\left(v_1 \frac{\partial}{\partial x_1} + v_2 \frac{\partial}{\partial x_2}\right) v_2 = -\frac{1}{\rho}\frac{\partial p}{\partial x_2} + \frac{\mu}{\rho}\nabla^2 v_2, \tag{2.2.5}$$

$$0 = -\frac{1}{\rho}\frac{\partial p}{\partial x_3} \tag{2.2.6}$$

with boundary conditions

$$v_1|_{x_3=0} = v_1|_{x_3=b} = 0,$$

$$v_2|_{x_3=0} = v_2|_{x_3=b} = 0,$$

where b is the gap between the two plates of the Hele-Shaw cell. Now we consider the case when b is sufficiently small and the flow is slow. Then, it is reasonable to neglect the derivatives with respect to x_1 and x_2 compared to those with respect to x_3;

$$\frac{\partial v_i}{\partial x_j} = 0, \quad \frac{\partial^2 v_i}{\partial {x_j}^2} = 0, \quad (i, j = 1, 2).$$

Hence equations (2.2.4) - (2.2.6) are rewritten as

$$\begin{aligned} \frac{\partial p}{\partial x_1} &= \mu \frac{\partial^2 v_1}{\partial {x_3}^2}, \\ \frac{\partial p}{\partial x_2} &= \mu \frac{\partial^2 v_2}{\partial {x_3}^2}, \\ 0 &= \frac{\partial p}{\partial x_3} \end{aligned}$$

Integrating the first two equations twice with boundary conditions above, we get

$$v_1 = -\frac{1}{2\mu} x_3 (b - x_3) \frac{\partial p}{\partial x_1},$$

$$v_2 = -\frac{1}{2\mu} x_3 (b - x_3) \frac{\partial p}{\partial x_2}.$$

The cross section of flows in the Hele-Shaw cell is parabolic which is known as the Poiseuille flow as shown in Fig.2.3. It is easy to get the mean value of flow over x_3

$$\tilde{v}_1 \equiv \frac{1}{b} \int_0^b v_1 \mathrm{d}x_3 = -\frac{b^2}{12\mu} \frac{\partial p}{\partial x_1},$$

$$\tilde{v}_2 \equiv \frac{1}{b} \int_0^b v_2 \mathrm{d}x_3 = -\frac{b^2}{12\mu} \frac{\partial p}{\partial x_2},$$

where $\tilde{v}_i$ is the integral mean of $v_i \, (i = 1, 2)$. Thus we obtain the governing equation for flows in the Hele-Shaw cell,

$$\tilde{\boldsymbol{v}} = -\frac{b^2}{12\mu} \nabla p. \tag{2.2.7}$$

Note that $\tilde{\boldsymbol{v}}$, the integral mean of $\boldsymbol{v}$, is the velocity vector for two-dimensional flow. Hereafter, we identify $\tilde{\boldsymbol{v}}$ with $\boldsymbol{v}$. Equation (2.2.7) is often referred to as the Hele-Shaw equation.

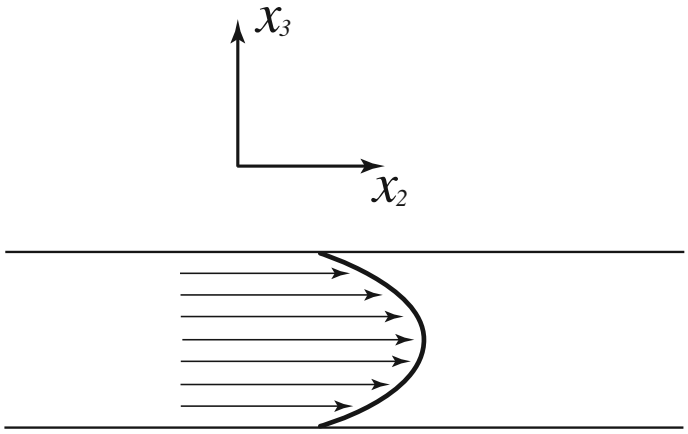

Figure 2.3: The cross section of a flow in the Hele-Shaw cell

2.2.2 Darcy's Law

The equation (2.2.7) reminds us of the Darcy's law, which is concerned with an averaged flow through a porous medium [45];

$$\bar{\boldsymbol{v}} = -\frac{k}{\mu}\nabla p, \tag{2.2.8}$$

where $\bar{\boldsymbol{v}}$ is a flux, which is defined as a fluid through a unit area at a unit time, k is the permeability of the medium, and μ is the viscosity of the fluid. This law was found experimentally in 1855 by Darcy, who was a French scientist and engineer [53]. In the two-dimensional case Darcy's law is the same form as the Hele-Shaw equation (2.2.7) with $k = b^2/12$, so that Eq. (2.2.7) is also referred to as the Darcy's law. Certainly, this law (2.2.8) resembles closely to the Hele-Shaw equation (2.2.7), however their origins are slightly different. As shown in the previous subsection, Hele-Shaw equation (2.2.7) is derived by averaging the flow with respect to x_3-direction. On the other hand, Darcy's law (2.2.8) represents the linear relationship between the macroscopically averaged flow and the pressure, which is analogous to the Ohm's law in the electrodynamics. In fact, if the porosity of the medium is statistically homogeneous, then the flow through the medium can be regarded as an ensemble of the microscopic Poiseuille flow, and hence this law holds. The more rigorous derivation can be found, for instance, in the work by Neuman [54].

Due to its simple formulation, Darcy's law is often used especially in the soil engineering in order to investigate, for instance, the flows of groundwater, and the enhanced oil recovery [55]. However, this law holds only within the linear regime for the averaged flow and the pressure. If the inertial term in the LHS of the Navier–Stokes equations (2.1.44) is taken into account,

the relationship between the flow and the pressure becomes

$$-\frac{\mu}{k}\bar{\boldsymbol{v}} - \frac{\rho}{k'}|\bar{\boldsymbol{v}}|^2 = \nabla p, \tag{2.2.9}$$

where k' denotes the inertial permeability. Equation (2.2.9) is known as Forchheimer equation, and also intensively investigated [56].

Chapter 3

Analytical Method

3.1 Hele-Shaw Problem and Laplace Equation

Now we consider two-phase Hele-Shaw problem, which is concerned with the motion of an interface between the fluid i $(i = 1, 2)$. As shown in the previous chapter, flows in a Hele-Shaw cell obey the following Darcy's law

$$\boldsymbol{v}_i = -\frac{b^2}{12\mu_i}\nabla p_i \quad (i = 1, 2), \tag{3.1.1}$$

where subindex i denotes the fluid i $(i = 1, 2)$. This implies $\nabla \times \boldsymbol{v}_i = 0$, so that there exists the velocity potential ϕ_i such that

$$\boldsymbol{v}_i = -\nabla\phi_i \quad (i = 1, 2). \tag{3.1.2}$$

Here we consider the case that the fluid is incompressible, *i.e.*,

$$\nabla \cdot \boldsymbol{v}_i = 0 \quad (i = 1, 2). \tag{3.1.3}$$

From Eqs. (3.1.2) and (3.1.3), the Laplace equation for ϕ is derived,

$$\nabla^2\phi_i = 0 \quad (i = 1, 2). \tag{3.1.4}$$

Thus, Hele-Shaw flows can be determined by solving the Laplace equations for ϕ_i under appropriate boundary conditions.

3.2 Free Boundary Problem and Boundary Conditions

3.2.1 Kinematic Boundary Condition

In general, an arbitrary surface $\mathscr{F}$ in the fluid is represented as $\mathcal{F}(\boldsymbol{x}, t) = 0$. Here we assume that the fluid particles on a surface at t remain on the same surface at any $t_1 > t$, which means,

$$\begin{aligned} \frac{\mathrm{D}\mathcal{F}}{\mathrm{D}t} &\equiv \frac{\partial \mathcal{F}}{\partial t} + \boldsymbol{v}_i \cdot \nabla \mathcal{F} \\ &= 0 \quad (i = 1, 2). \end{aligned} \tag{3.2.1}$$

Then, dividing both side by $|\nabla \mathcal{F}|\,(\neq 0)$ leads to

$$\frac{\partial \mathcal{F}/\partial t}{|\nabla \mathcal{F}|} + \boldsymbol{v}_i \cdot \frac{\nabla \mathcal{F}}{|\nabla \mathcal{F}|} = 0 \quad (i = 1, 2). \tag{3.2.2}$$

Since the unit normal vector $\mathbf{n}$ to the surface $\mathscr{F}$ is defined by $\nabla \mathcal{F}/|\nabla \mathcal{F}|$, then the normal velocity V of the surface $\mathscr{F}$ is defined by $(-1/|\nabla \mathcal{F}|)\,(\partial \mathcal{F}/\partial t)$ and

$$V = \boldsymbol{v}_i \cdot \mathbf{n}\,(i = 1, 2), \tag{3.2.3}$$

Eq. (3.2.1) or (3.2.3) is known as the kinematic boundary condition. This boundary condition is expected to hold for quite general cases, and employed in the most of free boundary problems.

3.2.2 Dynamical Boundary Condition

Along with the kinematic boundary condition, a dynamical boundary condition is employed in order to solve the Laplace equation. As the dynamical boundary condition, an equation about the pressure discontinuity at the interface is usually used. In general, this condition is derived for the case of a two-dimensional curved interface $\mathscr{F}$ in E^3 as follows.

Let us consider an interface $\mathscr{F}$ and an infinitesimal area D bounded by a closed contour ∂D on $\mathscr{F}$, as depicted in Fig. 3.1. Suppose that D' and $\partial D'$ are projections of D and ∂D to the tangential plane of $\mathscr{F}$ at some point O, respectively. Moreover, suppose that $\mathscr{F}$ is expressed as $x_3 = \mathcal{F}(x_1, x_2)$ around O and surface tension σ is constant on $\mathscr{F}$. Since the force acting on a side of the contour ∂D is

$$\begin{aligned} \mathrm{d}\boldsymbol{F} &= (-\sigma \mathbf{n}) \times \mathrm{d}\boldsymbol{x} \\ &= -\frac{\sigma}{\sqrt{1 + |\nabla \mathcal{F}|^2}} \left(-\mathcal{F}_{x_2}\mathrm{d}x_3 - \mathrm{d}x_2, \mathcal{F}_{x_1}\mathrm{d}x_3 + \mathrm{d}x_1, -\mathcal{F}_{x_1}\mathrm{d}x_2 + \mathcal{F}_{x_2}\mathrm{d}x_1\right) \end{aligned} \tag{3.2.4}$$

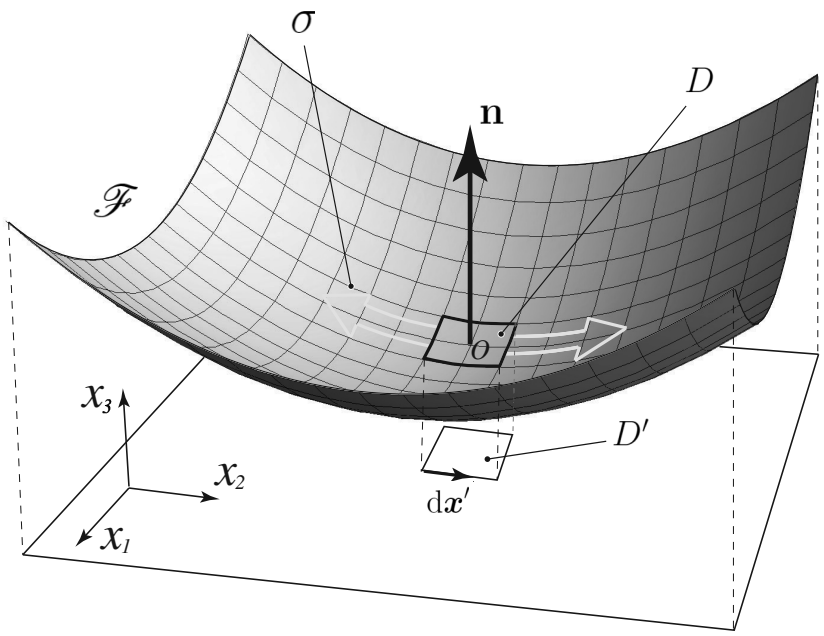

Figure 3.1: Forces acting on a curved interface

where $\mathrm{d}\boldsymbol{x} = (\mathrm{d}x_1, \mathrm{d}x_2, \mathrm{d}x_3)$ is the line element on ∂D, and the normal vector $\mathbf{n}$ is defined explicitly by

$$\mathbf{n} = \frac{1}{\sqrt{1+|\nabla\mathcal{F}|^2}}\,(-\mathcal{F}_{x_1}, -\mathcal{F}_{x_2}, 1), \tag{3.2.5}$$

whose the direction is toward the center of curvature, as seen in Fig. 3.1. In Eq. (3.2.4), subindex x_i of $\mathcal{F}$ denotes the derivative with respect to x_i $(i = 1, 2, 3)$.

If a domain D is sufficiently small, then D is well approximated by D', and hence $\mathrm{d}x_3 \approx 0$. Thus we have only to consider the x_3-component in Eq. (3.2.4). Therefore, the net force $\boldsymbol{F}$ acting on the area D is parallel to the x_3-axis, whose strength is

$$\begin{aligned} |\boldsymbol{F}| &= \oint_{\partial D} (-\sigma\mathbf{n}) \times \mathrm{d}\boldsymbol{x} \\ &\simeq -\sigma \oint_{\partial D'} \frac{(-\mathcal{F}_{x_1}\mathrm{d}x_2 + \mathcal{F}_{x_2}\mathrm{d}x_1)}{\sqrt{1+|\nabla\mathcal{F}|^2}} \\ &\simeq -\sigma \oint_{\partial D'} \frac{(\mathcal{F}_{x_2}, -\mathcal{F}_{x_1})}{\sqrt{1+|\nabla\mathcal{F}|^2}} \cdot \mathrm{d}\boldsymbol{x}' \end{aligned} \tag{3.2.6}$$

where $\mathrm{d}\boldsymbol{x}'$ is the line element on $\partial D'$. By using the Stokes' theorem, Eq. (3.2.6) can be transformed as

$$|\boldsymbol{F}| \simeq -\sigma \int_{D'} \nabla \times \frac{(\mathcal{F}_{x_2}, -\mathcal{F}_{x_1})}{\sqrt{1+|\nabla\mathcal{F}|^2}} \cdot \mathrm{d}\boldsymbol{S}'. \tag{3.2.7}$$

Therefore, in general, the net force for the interface $\mathscr{F}$ expressed by $\mathcal{F}(\boldsymbol{x}, t) = 0$ is

$$\begin{aligned} |\boldsymbol{F}| &\simeq -\sigma \int_D (\nabla \cdot \mathbf{n}) \, \mathrm{d}S \\ &= -\sigma K \delta S, \end{aligned} \tag{3.2.8}$$

where $K = \nabla \cdot \mathbf{n}$ denotes the total curvature, and δS represents the area of D. Equation (3.2.8) means that a domain on the interface is subjected to the force σK per unit area, caused by the surface tension. Therefore, for a static interface between the inner fluid (fluid 1) and the outer fluid (fluid 2), balance of the forces acting on the domain D can be written as

$$p_1 \delta S - \sigma K \delta S = p_2 \delta S \tag{3.2.9}$$

Thus, for a unit area, Young–Laplace equation can be derived as

$$p_1 - p_2 = \sigma K. \tag{3.2.10}$$

This equation (3.2.10) expresses that surface tension causes the pressure discontinuity, and the difference is determined by the curvature of the interface. This coincides with what are experimentally observed.

For the case of the Hele-Shaw problem, the right hand side of Eq. (3.2.10) is rewritten as

$$p_1 - p_2 = \sigma \left(\frac{2}{b} + H \right), \tag{3.2.11}$$

by considering the cell is thin enough. Here b denotes the thickness of the gap of the Hele-Shaw cell, and H is the two-dimensional curvature in the plane parallel to the Hele-Shaw cell.

Equation (3.2.11) has been used in common in the most studies for Hele-Shaw problem. However, it should be emphasized that Young–Laplace equation (3.2.10) is derived from an assumption that a static interface is in an equilibrium state. Therefore, for a dynamic interface, or nonequilibrium system, the derivation above does not always hold. In fact the validity of Young–Laplace equation has been studied [14, 15, 57]. There, the corrections to the Young–Laplace equation are investigated. The more detailed discussions are seen in Chapters 4 and 5.

3.3 Our Model and the Mode Coupling Equation

3.3.1 Theoretical Model for Hele-Shaw Problem

In this subsection, a theoretical model for radial Hele-Shaw problem is introduced by following the previous studies due to Paterson [19], and Miranda and Widom [44]. Let the system

be composed of two immiscible, incompressible viscous fluids in a Hele-Shaw cell. Hereafter $\boldsymbol{v}_i = \boldsymbol{v}_i(r, \theta, t)$, $p_i = p_i(r, \theta, t)$ and ∇ represent, respectively, the velocity vector, and the pressure of fluids $i = 1$ and 2, and the differential operator in the polar coordinates (r, θ).

The schematic configuration of the Hele-Shaw cell and the interface is depicted in Fig. 3.2. Here b is the thickness of the gap of the Hele-Shaw cell, and μ_1 and μ_2 denote the dynamic

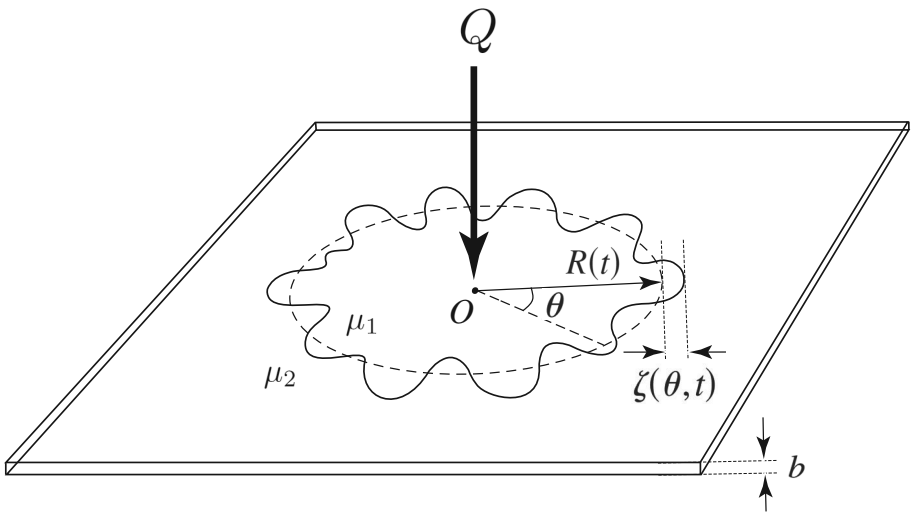

Figure 3.2: The Hele-Shaw cell and interface of fluids

viscosity coefficients of the inner $(i = 1)$ and the outer $(i = 2)$ fluids, respectively. It is known that the Saffman–Taylor instability occurs only when $\mu_1 < \mu_2$ [12]. Imagine that fluid 1 is injected with a constant rate Q from the centre O into the cell which was initially filled with fluid 2. Let the unperturbed interface at $t > 0$ be a circle of radius $R(t)$ with a centre O and the initial interface that of $R(t = 0) = R_0$, so that

$$R(t) = \sqrt{R_0^2 + \frac{Q}{\pi}t}. \tag{3.3.1}$$

Then the perturbed interface can be represented as

$$\mathcal{R} = R(t) + \zeta(\theta, t) \tag{3.3.2}$$

with the interface perturbation amplitude $\zeta(\theta, t)$, where θ is the polar angle.

3.3.2 Kinematic Boundary Condition in Our Model

The backgrounds and the model for theoretical studies of the Hele-Shaw problem have been almost prepared. Now, as a last step of preparations, useful analytical method for Hele-Shaw

problem is introduced. Miranda and Widom carried out first the weakly nonlinear analysis in [44]. There, they derived mode coupling equation introduced below, which is a nonlinear ordinary differential equation for perturbation of an interface. One of the merits of their analysis is that the time evolution of a perturbed interface is directly calculated based on the mode coupling equation. This is quite convenient to study the pattern formation for radial fingering phenomena. Following the argument due to Miranda and Widom, we derive of the mode coupling equation in this subsection.

As explained in the previous sections, the problem to be solved consists of Laplace equations $\nabla^2\phi_i = 0$ $(i = 1, 2)$ and two boundary conditions: the kinematic boundary condition and the Young–Laplace equation for the interface $\mathcal{R}$.

Due to Miranda and Widom [44], the general solutions of Laplace equations (3.1.4) are given by the Fourier power series as follows:

$$\phi_1 = {\phi_1}^0 + \sum_{n\neq 0} \phi_{1n}(t) \left(\frac{r}{R}\right)^{|n|} \mathrm{e}^{\mathrm{i}n\theta}, \quad (0 \leq r \leq \mathcal{R}) \tag{3.3.3}$$

$$\phi_2 = {\phi_2}^0 + \sum_{n\neq 0} \phi_{2n}(t) \left(\frac{R}{r}\right)^{|n|} \mathrm{e}^{\mathrm{i}n\theta}, \quad (\mathcal{R} \leq r) \tag{3.3.4}$$

with

$$\phi_i^0 = -\frac{Q}{2\pi} \log\left(\frac{r}{R}\right) + C_i \quad (i = 1, 2), \tag{3.3.5}$$

where C_i denotes the constant independent of both r and θ. Similarly, the interface perturbation amplitude $\zeta(\theta, t)$ is represented in terms of the Fourier power series

$$\zeta(\theta, t) = \sum_{n=-\infty}^{\infty} \zeta_n(t) \mathrm{e}^{\mathrm{i}n\theta}. \tag{3.3.6}$$

Here it is required that $\zeta_0(t)$ satisfies the following constraint

$$\zeta_0(t) = -\frac{1}{R(t)} \sum_{n\neq 0} |\zeta_n(t)|^2, \tag{3.3.7}$$

derived from the condition that the area $S = \pi R(t)^2$ of the fluid 1 is conserved independent of the perturbation $\zeta(\theta, t)$.

In order to derive a time evolution equation for perturbation $\zeta_n(t)$, Eqs. (3.3.3)-(3.3.6) should be substituted into boundary conditions. Since the interface grows radially, it is convenient to carry out all calculations in the two-dimensional polar coordinate system. Then the kinematic boundary condition (3.2.3) is written as follows:

$$\frac{\partial \mathcal{R}}{\partial t} = \left[\frac{1}{r^2}\frac{\partial \mathcal{R}}{\partial \theta}\frac{\partial \phi_i}{\partial \theta} - \frac{\partial \phi_i}{\partial r}\right]_{r=\mathcal{R}} \quad (i = 1, 2). \tag{3.3.8}$$

Substituting (3.3.3) and (3.3.4) into (3.3.8), we have up to the second order in ζ for ϕ_1

$$\begin{aligned}\frac{Q}{2\pi R}+\dot{\zeta} &= \frac{1}{R^2}\zeta_\theta\sum_{n\neq 0}(\mathrm{i}n)\phi_{1n}\mathrm{e}^{\mathrm{i}n\theta}+\frac{1}{R^3}\zeta\zeta_\theta\sum_{n\neq 0}(\mathrm{i}n)(|n|-2)\phi_{1n}\mathrm{e}^{\mathrm{i}n\theta}\\ &\quad+\frac{Q}{2\pi R}\left(1-\frac{\zeta}{R}+\frac{\zeta^2}{R^2}\right)\\ &\quad-\frac{1}{R}\sum_{n\neq 0}|n|\phi_{1n}\left(1+(|n|-1)\frac{\zeta}{R}+\frac{1}{2}(|n|-1)(|n|-2)\frac{\zeta^2}{R^2}\right)\mathrm{e}^{\mathrm{i}n\theta}, \quad (3.3.9)\end{aligned}$$

and for ϕ_2

$$\begin{aligned}\frac{Q}{2\pi R}+\dot{\zeta} &= \frac{1}{R^2}\zeta_\theta\sum_{n\neq 0}(\mathrm{i}n)\phi_{2n}\mathrm{e}^{\mathrm{i}n\theta}+\frac{1}{R^3}\zeta\zeta_\theta\sum_{n\neq 0}(\mathrm{i}n)(-|n|-2)\phi_{2n}\mathrm{e}^{\mathrm{i}n\theta}\\ &\quad+\frac{Q}{2\pi R}\left(1-\frac{\zeta}{R}+\frac{\zeta^2}{R}\right)\\ &\quad+\frac{1}{R}\sum_{n\neq 0}|n|\phi_{2n}\left(1-(|n|+1)\frac{\zeta}{R}+\frac{1}{2}(|n|+1)(|n|+2)\frac{\zeta^2}{R^2}\right)\mathrm{e}^{\mathrm{i}n\theta}, \quad (3.3.10)\end{aligned}$$

since $R_t = Q/2\pi R$. The dot over t means the time derivative and the subindex of ζ_θ the differentiation with respect to θ. Now let us express (3.3.8) in the form $\mu_1\phi_1 \pm \mu_2\phi_2$ up to the second order in ζ. Adding (3.3.9) multiplied by μ_1 and (3.3.10) multiplied by μ_2 and making use of (3.3.6), we deduce for $n \neq 0$

$$\begin{aligned}\mu_1\phi_{1n}+\mu_2\phi_{2n} &= -\frac{R}{|n|}(\mu_1-\mu_2)\dot{\zeta}_n-(\mu_1-\mu_2)\frac{Q}{2\pi R|n|}\zeta_n\\ &\quad+(\mu_1+\mu_2)\sum_{n'\neq 0}\mathrm{sgn}(nn')\left(\dot{\zeta}_{n'}\zeta_{n-n'}+\frac{Q}{2\pi R^2}\zeta_{n'}\zeta_{n-n'}\right)\\ &\quad-(\mu_1-\mu_2)\sum_{n'\neq 0}\frac{1}{|n|}\dot{\zeta}_{n'}\zeta_{n-n'}, \quad (3.3.11)\end{aligned}$$

where $\mathrm{sgn}(nn')$ is the sign function defined by

$$\mathrm{sgn}(nn') = \begin{cases} 1 & (nn'>0),\\ -1 & (nn'<0).\end{cases}$$

Similarly, by subtracting (3.3.10) multiplied by μ_2 from (3.3.9) multiplied by μ_1, it is obtained

$$\begin{aligned}\mu_1\phi_{1n} - \mu_2\phi_{2n} &= -\frac{R}{|n|}(\mu_1+\mu_2)\dot{\zeta}_n - (\mu_1+\mu_2)\frac{Q}{2\pi R|n|}\zeta_n \\ &\quad +(\mu_1-\mu_2)\sum_{n'\neq 0}\mathrm{sgn}(nn')\left(\dot{\zeta}_{n'}\zeta_{n-n'} + \frac{Q}{2\pi R^2}\zeta_{n'}\zeta_{n-n'}\right) \\ &\quad -(\mu_1+\mu_2)\sum_{n'\neq 0}\frac{1}{|n|}\dot{\zeta}_{n'}\zeta_{n-n'}. \end{aligned} \tag{3.3.12}$$

3.3.3 Dynamical Boundary Condition in Our Model

Similarly in the previous subsection, Eqs. (3.3.3)-(3.3.6) are substituted into Young–Laplace equation

$$p_1 - p_2 = \sigma\left(\frac{2}{b} + H\right). \tag{3.2.11}$$

It is well-known that the curvature H can be explicitly calculated from the unit normal vector $\mathbf{n}$ to the interface $\mathcal{R}$

$$\mathbf{n} = ((\mathbf{n})_r, (\mathbf{n})_\theta) = \left.\frac{1}{\sqrt{r^2+r_\theta^2}}(r, -r_\theta)\right|_{r=\mathcal{R}}. \tag{3.3.13}$$

Here and in what follows $(\cdot)_r$ and $(\cdot)_\theta$ are the r- and θ-component of $(\cdot)$, respectively. In addition, because of Darcy's law the relationships between p_i and ϕ_i are

$$p_i = \frac{12\mu_i}{b^2}\phi_i \quad (i=1,2). \tag{3.3.14}$$

Therefore, by substituting Eqs. (3.3.3)-(3.3.6) with Eqs. (3.3.13) and (3.3.14) into Young–Laplace equation (3.2.11), and it is obtained as

$$\begin{aligned}&\frac{12}{b^2}\left\{(\mu_1-\mu_2)\left(-\frac{Q}{2\pi}\right)\left(\xi - \frac{1}{2}\xi^2\right) + \sum_{n\neq 0}\left[(\mu_1\phi_{1n} - \mu_2\phi_{2n}) + |n|\xi(\mu_1\phi_{1n} + \mu_2\phi_{2n})\right]\right\} \\ &= \sigma\left[\frac{2}{b} + \frac{1}{R}\left\{1 - (\xi + \xi_{\theta\theta}) + \left(\xi^2 + \frac{1}{2}\xi_\theta^2 + 2\xi\xi_{\theta\theta}\right)\right\}\right], \end{aligned} \tag{3.3.15}$$

where $\xi = \zeta/R$ for convenience.

As indicated before, the validity of Young–Laplace equation has been discussed and investigated in [14, 15, 20, 57]. There are two contexts of researches to modify Young–Laplace equation; the one taking the viscous normal stress terms into consideration due to Kim *et al.* [57], and the other taking into account the effects of a wetting layer in the Hele-Shaw cell which

is proposed by Park and Homsy [15]. In fact, Miranda and co-authors also reported analytical results by employing corrected Young–Laplace equation in their recent studies [58, 59]. However, for instance in [58], the corrected terms seem to be not enough from the theoretical point of views. On the other hand, there appears to be corrected to excess in [59]. Putting off further discussions about these points to the following chapters, in the rest of this chapter we derives the mode coupling equation based on the basic Young–Laplace equation.

3.3.4 Mode Coupling Equation

Substituting (3.3.11) and (3.3.12) into the left hand side of (3.3.15) and keeping up to the quadratic terms in ζ, we obtain

$$\begin{aligned}
\dot{\zeta}_n &= \left\{ \frac{Q}{2\pi R^2}(A|n|-1) - \frac{\alpha}{R^3}|n|(n^2-1) \right\} \zeta_n \\
&\quad + \sum_{n' \neq 0} \frac{|n|}{R} \left\{ \frac{QA}{2\pi R^2} \left(\frac{1}{2} - \mathrm{sgn}(nn') \right) - \frac{\alpha}{R^3} \left(1 - \frac{n'}{2}(3n'+n) \right) \right\} \zeta_{n'} \zeta_{n-n'} \\
&\quad + \sum_{n' \neq 0} \frac{1}{R} \left\{ A|n| \left(1 - \mathrm{sgn}(nn') \right) - 1 \right\} \dot{\zeta}_{n'} \zeta_{n-n'}, \qquad (3.3.16)
\end{aligned}$$

where parameters are defined as

$$\begin{aligned}
A &= \frac{\mu_2 - \mu_1}{\mu_2 + \mu_1}, \\
\alpha &= \frac{b^2 \sigma}{12(\mu_1 + \mu_2)}.
\end{aligned}$$

The principal term of Eq. (3.3.16) is a linear part

$$\dot{\zeta}_n = \left\{ \frac{Q}{2\pi R^2}(A|n|-1) - \frac{\alpha}{R^3}|n|(n^2-1) \right\} \zeta_n. \qquad (3.3.17)$$

By substituting Eq. (3.3.17) into the last term in the right hand side of Eq. (3.3.16), then Eq. (3.3.16) is rewritten as

$$\dot{\zeta}_n = \lambda(n)\zeta_n + \sum_{n' \neq 0} \gamma(n, n') \zeta_{n'} \zeta_{n-n'}, \qquad (3.3.18)$$

which is equivalent to Eq. (3.3.16) within the second order in ζ_n, where

$$\lambda(n) = \frac{Q}{2\pi R^2}(A|n| - 1) - \frac{\alpha}{R^3}|n|(n^2 - 1), \tag{3.3.19}$$

$$\begin{aligned}\gamma(n, n') = \frac{1}{R}\Bigg[&\frac{Q}{2\pi R^2}\left\{A|n|\left(A|n'|(1 - \mathrm{sgn}(nn')) - \frac{1}{2}\right) - (A|n'| - 1)\right\} \\ &-\frac{\alpha}{R^3}\left\{|n|\left(1 - \frac{1}{2}nn' - \frac{3}{2}n'^2\right) + (A|n|(1 - \mathrm{sgn}(nn')) - 1)\,|n'|(n'^2 - 1)\right\}\Bigg].\end{aligned} \tag{3.3.20}$$

Equation (3.3.18) with Eqs. (3.3.19) and (3.3.20) is also referred to as the mode coupling equation [44]. In Eq. (3.3.18), $\lambda(n)$ and $\gamma(n, n')$ express the linear growth of perturbation ζ_n and the strength of coupling with other modes, respectively. In the following chapters, we see how the original mode coupling equation (3.3.18) is modified by the correction to Young–Laplace equation.

Chapter 4

Weakly Nonlinear Analysis with the Effect of Viscous Normal Stress

In the previous chapter, it was indicated that the validity of Young–Laplace equation (3.2.11) has been controversial, for instance, in [14, 15, 20, 57, 58]. In this Chapter we introduce the improvement of Young–Laplace equation, and derive the new mode coupling equation based on this improved Young–Laplace equation. Then weakly nonlinear analysis is carried out, and the numerical results are shown, which are the extension of the previous studies due to Miranda and co-authors [44, 58].

4.1 Balance of Normal Stress

4.1.1 Validity of Young–Laplace Equation

As mentioned previously, the effort to improve Young–Laplace equation has been still continued. Young–Laplace equation was employed first in the pioneering work due to Saffman and Taylor [12] and Chouke *et al.* [13], and widely used in the almost all later investigations [19, 44]. However, as emphasized before, it seems to be inappropriate as a boundary condition for Hele-Shaw problem.

One of the reasons is a discrepancy between the theoretical and experimental results about the widths of the Saffman–Taylor finger in rectangular Hele-Shaw cells. Let the ratio of the width of the finger to the width of the cell be λ. As mentioned in Chapter 1, Saffman and Tay-

lor experimentally revealed that λ is selected to be $1/2$ for a Saffman–Taylor finger, however, the value of λ remains undetermined analytically in the case that the surface tension effect is important [12]. After then McLean and Saffman proceeded the Saffman–Taylor's analysis in [14], and obtained the dependence of λ on the surface tension parameter, which qualitatively agrees with observation. However, their numerical results seemed not to satisfy the quantitative agreement; they indicated that this is caused by employing Young–Laplace equation, and suggested the modified form of the boundary condition.

Another reason seems to be simpler and more essential; Young–Laplace equation is derived from the balance of the net force for a static interface, as shown in subsection 3.2.2. There is no guarantee that this equation also holds for a dynamic interface or a nonequilibrium system, where the balance of static pressure and surface tension does not always hold. In fact, a boundary condition for the dynamic interface has been addressed in [45, 60]. They remarked that the balance of stress should be considered instead of Young–Laplace equation.

4.1.2 Balance of Normal Stress

Let $\mathbf{T}_i$ be stress tensors for fluid i. Then, the normal stress balance at the interface between fluids 1 and 2 is

$$\mathbf{n} \cdot \mathbf{T}_2 \cdot \mathbf{n} - \mathbf{n} \cdot \mathbf{T}_1 \cdot \mathbf{n} = \sigma \left(\frac{2}{b} + H \right). \tag{4.1.1}$$

For the case of Newtonian fluid, stress tensors have been already derived in subsection 2.1.5 as

$$\mathbf{T}_i = -p_i \mathbf{I} + 2\mu_i \mathbf{e}_i \quad (i = 1, 2) \tag{4.1.2}$$

with $\mathbf{e}_i$ being the rate of strain tensor for fluid i whose (j,k)-component $(\mathbf{e}_i)_{jk}$ is given as

$$(\mathbf{e}_i)_{jk} = \frac{1}{2} \left(\frac{\partial (\boldsymbol{v}_i)_j}{\partial x_k} + \frac{\partial (\boldsymbol{v}_i)_k}{\partial x_j} \right) \quad (j, k = 1, 2). \tag{4.1.3}$$

Here the index j of $(\cdot)_j$ means the j-component with respect to the two dimensional Cartesian coordinates (x_1, x_2), respectively. The curvature H is supposed to be negative for the convex domain.

Then the normal stress balance (4.1.1) can be written simply as

$$p_1 - p_2 + [2\mu_1 \mathbf{n} \cdot \mathbf{e}_1 \cdot \mathbf{n} - 2\mu_2 \mathbf{n} \cdot \mathbf{e}_2 \cdot \mathbf{n}]_{r=\mathcal{R}} \;=\; \sigma \left(\frac{2}{b} + H \right). \tag{4.1.4}$$

It is clear that Eq. (4.1.4) is the more general boundary condition than Young–Laplace equation (3.2.11). Actually, if each of fluids moves without deformation, in other words $\mathbf{e}_i = 0$ $(i = 1, 2)$,

then the balance of the normal stress (4.1.4) reduces to Young–Laplace equation (3.2.11). Therefore, it seems to be reasonable to employ the normal stress balance (4.1.4) for a dynamic case.

This boundary condition (4.1.4) has not been paid much attention except for the work by Kim *et al.* [57]. In [57], the third and fourth terms in the left hand side of Eq. (4.1.4) were referred to as viscous normal stress. Hereafter, following Kim *et al.*, we also refer to these terms as viscous normal stress, or shortly, VNS. By employing Eq. (4.1.4), they attained the more satisfactory results than the previous results in [15, 20]. They also referred to the splitting of fingers, however, their main topic was not in the context of pattern formation and morphology of interfaces. Moreover, their work [57] was limited to the linear analysis, which is applicable only to the earlier stage of fingering phenomena , and did not give us enough answer to the patten formed by an unstable interface.

Recently, Gadêlha and Miranda [58] carried out weakly nonlinear analysis based on the normal stress balance (4.1.4). However, their boundary condition is not complete; only a part of VNS terms is included. Therefore, as a next step, it is quite natural to develop the nonlinear analysis based on the normal stress balance properly. In the following section, we proceed with employing Eq. (4.1.4), which contains the VNS terms completely as reported in [61].

4.2 Extended Mode Coupling Equation

In this section, the mode coupling equation taking the effect of VNS terms into account is considered. The model for radial Hele-Shaw problem was shown in Fig. 3.2.

In the polar coordinates, the components of $\mathbf{e}_i$ are given as follows:

$$
\begin{aligned}
(\mathbf{e}_i)_{rr} &= \frac{\partial(\boldsymbol{v}_i)_r}{\partial r}, \\
(\mathbf{e}_i)_{r\theta} &= (\mathbf{e}_i)_{\theta r} = \frac{r}{2}\frac{\partial}{\partial r}\frac{(\boldsymbol{v}_i)_\theta}{r} + \frac{1}{2r}\frac{\partial(\boldsymbol{v}_i)_r}{\partial\theta}, \\
(\mathbf{e}_i)_{\theta\theta} &= \frac{1}{r}\frac{\partial(\boldsymbol{v}_i)_\theta}{\partial\theta} + \frac{(\boldsymbol{v}_i)_r}{r} \quad (i = 1, 2).
\end{aligned}
$$

Accordingly, Eq. (4.1.4) becomes

$$
\begin{aligned}
p_1 - p_2 \;&+\; 2\mu_1 \left[(\mathbf{n})_r^2 \frac{\partial^2 \phi_1}{\partial r^2} + (\mathbf{n})_r (\mathbf{n})_\theta \left(\frac{1}{r} \frac{\partial^2 \phi_1}{\partial r \partial \theta} - \frac{1}{r^2} \frac{\partial \phi_1}{\partial \theta} \right) + (\mathbf{n})_\theta^2 \left(\frac{1}{r^2} \frac{\partial^2 \phi_1}{\partial \theta^2} + \frac{1}{r} \frac{\partial \phi_1}{\partial r} \right) \right]_{r=\mathcal{R}} \\
&-\; 2\mu_2 \left[(\mathbf{n})_r^2 \frac{\partial^2 \phi_2}{\partial r^2} + (\mathbf{n})_r (\mathbf{n})_\theta \left(\frac{1}{r} \frac{\partial^2 \phi_2}{\partial r \partial \theta} - \frac{1}{r^2} \frac{\partial \phi_2}{\partial \theta} \right) + (\mathbf{n})_\theta^2 \left(\frac{1}{r^2} \frac{\partial^2 \phi_2}{\partial \theta^2} + \frac{1}{r} \frac{\partial \phi_2}{\partial r} \right) \right]_{r=\mathcal{R}} \\
&=\; \sigma \left(\frac{2}{b} + \frac{r^2 + 2r_\theta^2 - r r_{\theta\theta}}{(r^2 + r_\theta^2)^{3/2}} \right)_{r=\mathcal{R}} \qquad (4.2.1)
\end{aligned}
$$

with ϕ_1 and ϕ_2 being given by (3.3.3) and (3.3.4), respectively. Here we emphasize that the condition (4.2.1) includes the complete VNS effect, in comparison with the one in [58].

The following process is similar to the case of the original mode coupling equation. Since p_i are related with ϕ_i by Eq. (3.3.14), we obtain by substituting Eqs. (3.3.12) and (3.3.11) into Eq. (4.2.1),

$$
\begin{aligned}
\{1 + 2\epsilon|n|(A + |n|)\}\, \dot{\zeta}_n \;&=\; \left\{ \frac{Q}{2\pi R^2}(A|n| - 1) - \frac{\alpha}{R^3}|n|(n^2 - 1) + \epsilon \frac{Q}{\pi R^2}(A|n| - n^2) \right\} \zeta_n \\
&+ \sum_{n' \neq 0} \frac{|n|}{R} \left\{ \frac{QA}{2\pi R^2} \left(\frac{1}{2} - \mathrm{sgn}(nn') \right) - \frac{\alpha}{R^3} \left(1 - \frac{n'}{2}(3n' + n) \right) \right. \\
&\quad \left. - \epsilon \frac{Q}{\pi R^2} \left(A(3nn' - 4n'^2 + 1) + |n|(A|n| + 1)\mathrm{sgn}(nn') - \frac{n'}{|n'|}(4n' - n) \right) \right\} \zeta_{n'} \zeta_{n-n'} \\
&+ \sum_{n' \neq 0} \frac{1}{R} \left\{ A|n| \left(1 - \mathrm{sgn}(nn')\right) - 1 - 2\epsilon|n| \left\{ |n|(A|n| + 1)\mathrm{sgn}(nn') \right. \right. \\
&\quad \left. \left. + (A + |n|) - \frac{n'}{|n'|}(4n' - n) + A|n'|(2n'^2 - nn' + 2) \right\} \dot{\zeta}_{n'} \zeta_{n-n'}. \right.
\end{aligned}
$$

Parameter ϵ introduced here represents the effect of VNS defined by

$$
\epsilon \;=\; \epsilon(t) = \frac{b^2}{12} \frac{1}{R(t)^2}. \qquad (4.2.2)
$$

In addition let the Hele-Shaw cell be so thin (*i.e.*, $\epsilon \ll 1$) that we can use an approximation

$$
\{1 - 2\epsilon|n|(A + |n|)\}^{-1} \simeq 1 + 2\epsilon|n|(A + |n|).
$$

Then, keeping the first order term in ϵ, we finally obtain the time evolution equation for the perturbation amplitude $\zeta_n(t)$:

$$
\frac{\partial \zeta_n}{\partial t} \equiv \dot{\zeta}_n = \Lambda(n)\zeta_n + \sum_{n' \neq 0} \Gamma(n, n') \zeta_{n'} \zeta_{n-n'}, \qquad (4.2.3)
$$

where

$$\Lambda(n) = \frac{Q}{2\pi R^2}(A|n|-1) - \frac{\alpha}{R^3}|n|(n^2-1) + \epsilon n^2 \frac{Q}{\pi R^2}(A|n| - A^2 - 2) + 2\epsilon \frac{\alpha}{R^3} n^2(n^2-1)(A+|n|), \tag{4.2.4}$$

$$\begin{aligned}
\Gamma(n,n') = {} & \frac{1}{R}\left[\frac{Q}{2\pi R^2}\left(A|n|\left\{A|n'|(1-\mathrm{sgn}(nn')) - \frac{1}{2}\right\} - (A|n'|-1)\right)\right. \\
& \left. -\frac{\alpha}{R^3}\left(|n|\left(1 - \frac{1}{2}nn' - \frac{3}{2}n'^2\right) + \{A|n|(1-\mathrm{sgn}(nn')) - 1\}|n'|(n'^2-1)\right)\right] \\
& + \frac{\epsilon}{R}\left[-\frac{Q}{\pi R^2}\left(An^2|n'|(1-A^2)\mathrm{sgn}(nn') + A|n|\left\{-4n'^2(n'+1) + \frac{1}{2}|n|(A+|n|+4n') + 1\right\}\right.\right. \\
& \qquad + A|n|(A|n'|-1)\left\{|n|(A+|n|) + |n'|(2n'^2 - nn' + 2)\right\} \\
& \qquad \left. - n'^2(A|n'| - A^2 + 2)\{A|n|(1-\mathrm{sgn}(nn')) - 1\}\right) \\
& + 2\frac{\alpha}{R^3}\left(n^2(A+|n|)\left(1 - \frac{1}{2}nn' - \frac{3}{2}n'^2\right) + n^2|n'|(n'^2-1)(1-A^2)\mathrm{sgn}(nn')\right. \\
& \qquad + A|n||n'|(n'^2-1)\left\{|n|(A+|n|) + |n'|(2n'^2 - nn' + 2)\right\} \\
& \left.\left. - |n|n'(n'^2-1)(4n'-n) + n'^2(n'^2-1)(A+|n'|)\{A|n|(1-\mathrm{sgn}(nn')) - 1\}\right)\right].
\end{aligned} \tag{4.2.5}$$

Hereafter we refer to the Eq. (4.2.3) with Eqs. (4.2.4) and (4.2.5) as the extended mode coupling equation. As will be seen in the next section, $\Lambda(n)$ and $\Gamma(n,n')$ represent the linear growth rate and the coupling coefficient of the n-th mode perturbation amplitude, respectively. Note that both $\Lambda(n)$ and $\Gamma(n,n')$ are the extended formulae of those derived by Miranda and co-authors [44, 58] and Kim *et al.* [57] in the following sense. When $\epsilon = 0$, (4.2.4) and (4.2.5) are the same as those in [44, 58], while for the nonzero ϵ the effect of VNS is taken into consideration. Since ϵ is defined as Eq. (4.2.2), the terms with ϵ in Eqs. (4.2.4) and (4.2.5) represent the 3-dimensional variation of the interface, which was not taken into account in the previous studies [44, 58]. In comparison with those of Kim *et al.* theirs contain only one-Fourier mode, so that their result is only for the linear evolution, that is $\Gamma(n,n') = 0$. Thus we see that the extended mode coupling equation (4.2.3) is certainly a generalized one compared with those in the previous studies [44, 57, 58].

4.3 Analysis of the Results

In this section we analyze how these results with nonzero ϵ affect the behaviours of the interfaces. In the previous section we derived equation (4.2.3) for ζ_n, when the interface in problem was represented by the sum of the non-perturbed radius and the perturbation

$$\mathcal{R} = R(t) + \zeta(\theta, t), \tag{3.3.2}$$

$$\zeta(\theta, t) = \sum_{n=-\infty}^{\infty} \zeta_n(t) \mathrm{e}^{\mathrm{i}n\theta}. \tag{3.3.6}$$

Now we are at the stage to study the time evolution of the interface. First we consider the linear evolution, that is, (4.2.3) without $\Gamma(n, n')$. In this case the interface is merely a superposition of the n-th mode perturbation. Second we study (4.2.3) itself with nonlinear term. In this case, the behaviour of the interface becomes more complex because of the mode coupling of the nonlinear term in (4.2.3). We discuss the difference between the linear and the nonlinear evolutions, especially including the effect of the viscous normal stresses.

4.3.1 Linear Approximated Perturbation

The time evolution equation that we discuss in this subsection is as follows.

$$\dot{\zeta_n} = \Lambda(n)\zeta_n \tag{4.3.1}$$

with $\Lambda(n)$ being defined by (4.2.4). It is easy to see that the solution of (4.3.1) is given by

$$\zeta_n(t) = \zeta_n(0) \exp\left(\int_0^t \Lambda(n)\, \mathrm{d}t'\right).$$

Obviously if $\Lambda(n) < 0$, then $\zeta_n(t)$ decays with t and the interface remains stable; while, if $\Lambda(n) > 0$ the perturbation grows exponentially, which means the interface instability. By noting that Λ is dependent on $R(t)$, the instability condition is given by the relationship $R(t) > R_c(n)$, where the critical radius $R_c(n)$ is derived from the equation $\Lambda(n) = 0$,

$$R_c(n) = \frac{2\pi\alpha}{Q} \frac{|n|(n^2-1)\{1 - 2\epsilon|n|(A+|n|)\}}{A|n| - 1 + 2\epsilon n^2(A|n| - A^2 - 2)}.$$

It should be noted that the existence of $R_c(n)$ is guaranteed by the implicit function theorem. Hence up to the first order in ϵ, $R_c(n)$ is equal to

$$R_c(n) = \frac{2\pi\alpha}{Q} \frac{|n|(n^2-1)}{A|n| - 1} \left(1 - 2\epsilon|n| \frac{2An^2 - 3|n| - A}{A|n| - 1}\right). \tag{4.3.2}$$

In the pioneering work by Paterson [19], fluids 1 and 2 are air and glycerine, respectively, whose viscosities are $\mu_1 = 1.8 \times 10^{-5}\,\mathrm{g/(cm \cdot s)}$ and $\mu_2 = 5.21\,\mathrm{g/(cm \cdot s)}$, so that one can regard the Atwood number $A = (\mu_2 - \mu_1)/(\mu_2 + \mu_1)$ as $A = 1$.

Hereafter we proceed with our discussion under this assumption $A = 1$. Then (4.3.2) becomes

$$R_c(n) = \frac{2\pi\alpha}{Q}|n|(|n|+1)\left\{1 - 2\epsilon|n|\frac{2n^2 - 3|n| - 1}{|n| - 1}\right\}. \tag{4.3.3}$$

Following the argument in [44], we consider the following approximation of the solution of equation (4.3.1):

$$\zeta_n^{lin}(t) = \begin{cases} \zeta_n(0) & (R(t) < R_c(n)), \\ \zeta_n(0)\left(\dfrac{R}{R_c}\right)^{|n|-1+\epsilon f(n)} \exp\left[(|n| - 1 + \epsilon f(n))\left(\dfrac{R_c}{R} - 1\right)\right] & \\ & (R(t) > R_c(n)), \end{cases} \tag{4.3.4}$$

where $f(n) = 2n^2(|n|-3)$ represents the 3-dimensional effect due to the viscous normal stresses. In this aspect our result seems to be the natural extension of equation (28) in [44].

4.3.2 Weakly Nonlinear Evolution

In this subsection, based on the approximated solution (4.3.4) we consider the extended mode coupling equation (4.2.3). Again following Miranda and Widom [44], we consider equation (4.2.3) with the quadratic terms $\zeta_{n'}(t)\zeta_{n-n'}(t)$ replaced by $\zeta_{n'}^{lin}(t)\zeta_{n-n'}^{lin}(t)$, that is

$$\dot{\zeta_n} = \Lambda(n)\zeta_n + \Xi(n,t), \tag{4.3.5}$$

$$\Xi(n,t) = \sum_{n' \neq 0} \Gamma(n,n')\zeta_{n'}^{lin}(t)\zeta_{n-n'}^{lin}(t). \tag{4.3.6}$$

Here $\Lambda(n)$ and $\Gamma(n,n')$ are defined by (4.2.4) and (4.2.5), respectively. Due to Miranda and Widom [44], (4.3.5) can be approximately solved as

$$\zeta_n(t) = \begin{cases} \zeta_n(0) & (R(t) < R_c(n)), \\ \zeta_n^{lin}(t)\left\{1 + \displaystyle\int_{t_c(n)}^{t} \frac{\Xi(n,t')}{\zeta_n^{lin}(t')}\mathrm{d}t'\right\} & (R(t) > R_c(n)), \end{cases} \tag{4.3.7}$$

which corresponds to (32) in [44]. In (4.3.7) above $t_c(n)$ is defined as $R(t_c(n)) = R_c(n)$.

From the form of the linear approximated solution (4.3.4), it is obvious that $\zeta_n^{lin} = \zeta_{-n}^{lin}$ in (4.3.7). Therefore the approximated solution $\zeta(\theta, t)$ can be written without loss of generality as

$$\begin{aligned}
\zeta(\theta, t) &= \sum_{n=\infty}^{\infty} \zeta_n(t) \mathrm{e}^{\mathrm{i}n\theta} \\
&= \zeta_0 + \sum_{n\neq 0}^{\infty} \{(\zeta_n + \zeta_{-n})\cos(n\theta) + \mathrm{i}(\zeta_n - \zeta_{-n})\sin(n\theta)\} \\
&= \zeta_0 + 2\sum_{n\neq 0}^{\infty} \zeta_n \cos(n\theta),
\end{aligned}$$

so that the perturbed interface is approximated by

$$\mathcal{R} = R(t) + \zeta_0 + 2\sum_{n\neq 0}^{\infty} \zeta_n(t)\cos(n\theta).$$

Here ζ_0 is determined by the constraint (3.3.7).

Figures 4.1 and 4.2 depict the trajectories of $\mathcal{R}$ plotted with a variation of t. The parameters are the same as those used in Paterson's experiments, *i.e.*, $b = 0.15\,\mathrm{cm}$, $Q = 9.3\,\mathrm{cm}^3/\mathrm{s}$, $\sigma = 63\,\mathrm{dynes/cm}$ and $R_0 = 0.05\,\mathrm{cm}$ [19]. The initial perturbation is in the n-dependent random phase with amplitude $R_0/500$, which are the same as in [44]. Here the modes n are chosen as $n = 5$, 10, 15. It should be noted that this choice of n is not necessarily sufficient by considering the real phenomena, in which the other modes naturally exist. However, such a simplification is useful in order to clarify how the VNS terms affect the fingering patterns, especially the splitting of the fingers. Figure 4.1 depicts the time evolution of the perturbed interfaces without VNS effect, which is the same as the previous results based on the Young–Laplace equation (3.2.11). In Fig. 4.1, the dotted curves represent the interfaces at $t = 5$, 15 and 25 sec, while the solid curves represent the ones at $t = 10$, 20 and 30 sec, from the centre outward, respectively. One can see that the interface is nearly a circle until $t = 10\,\mathrm{sec}$, then it becomes unstable ($t = 15$, 20 sec) and some fingers grow ($t = 25$, 30 sec) in the figure. On the other hand, Fig. 4.2 shows the evolution of the interface with VNS effect, under the same parameters and initial conditions as Fig. 4.1. The time interval of each curve is also 5 sec. From these figures, one can recognize the qualitative difference between the cases with and without VNS; more fingers appear in Fig. 4.2, and some of them have wider tips than those in Fig. 4.1. Moreover, some tips of fingers in Fig. 4.1 appear to split into two in Fig. 4.2. This is also shown in Fig. 4.3, which the interfaces with and without VNS at $t = 30\,\mathrm{sec}$ are compared. These behaviours of the

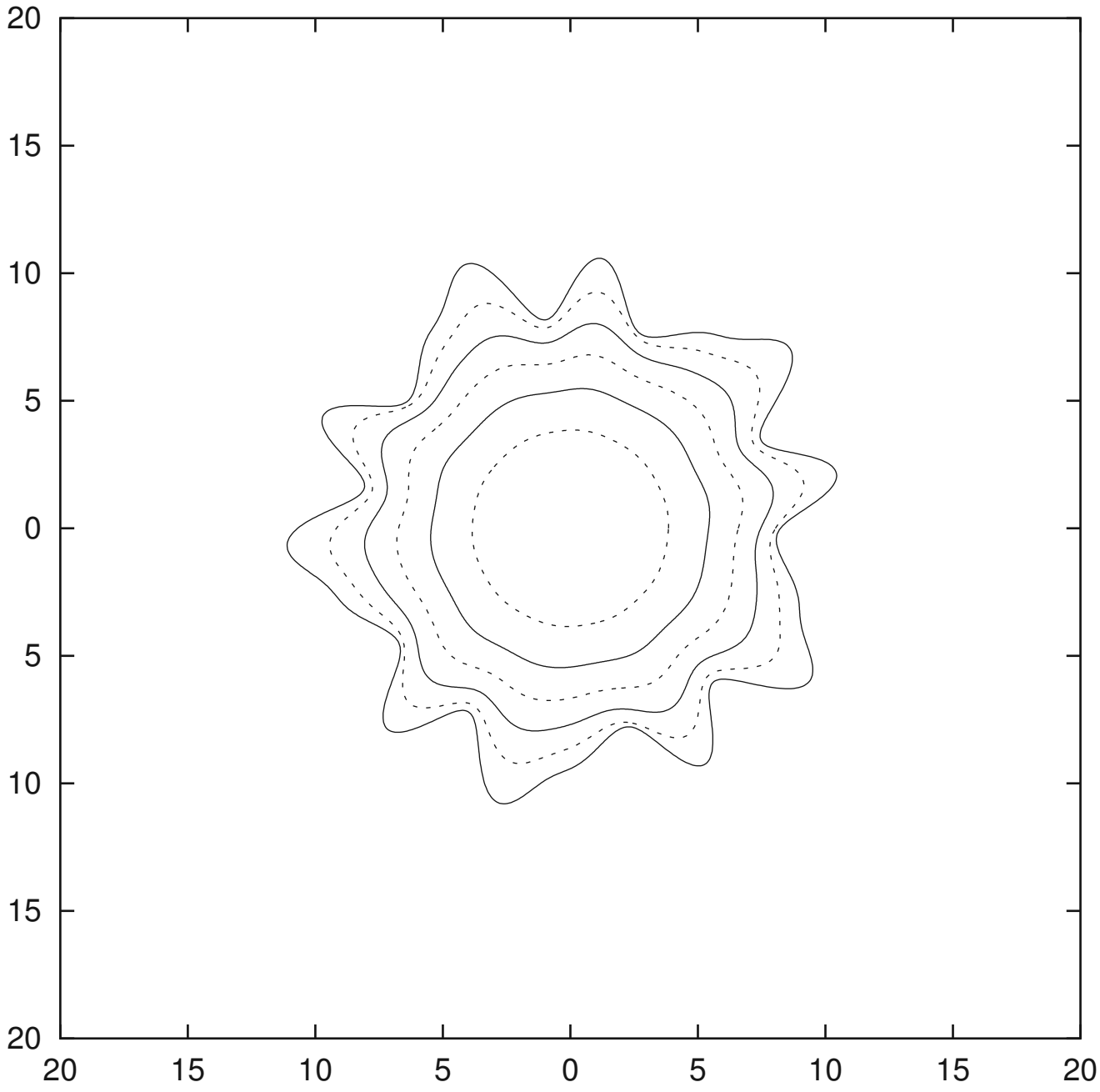

Figure 4.1: Interface growth without VNS from $t = 5$ to 30 sec. The modes are chosen as $n = 5$, 10, 15.

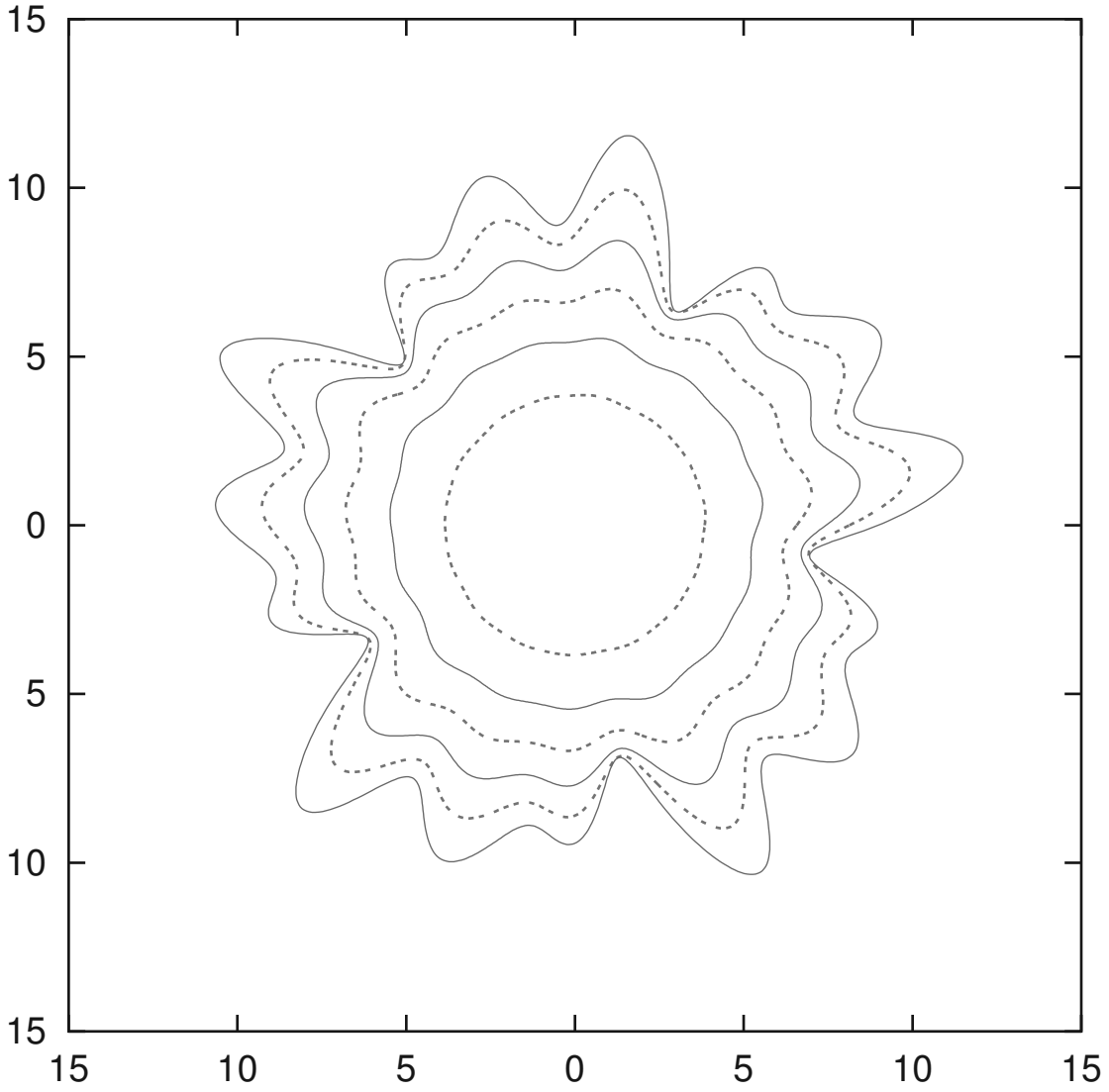

Figure 4.2: Interface growth with VNS from $t = 5$ to 30 sec. The modes are chosen as $n =$ 5, 10, 15.

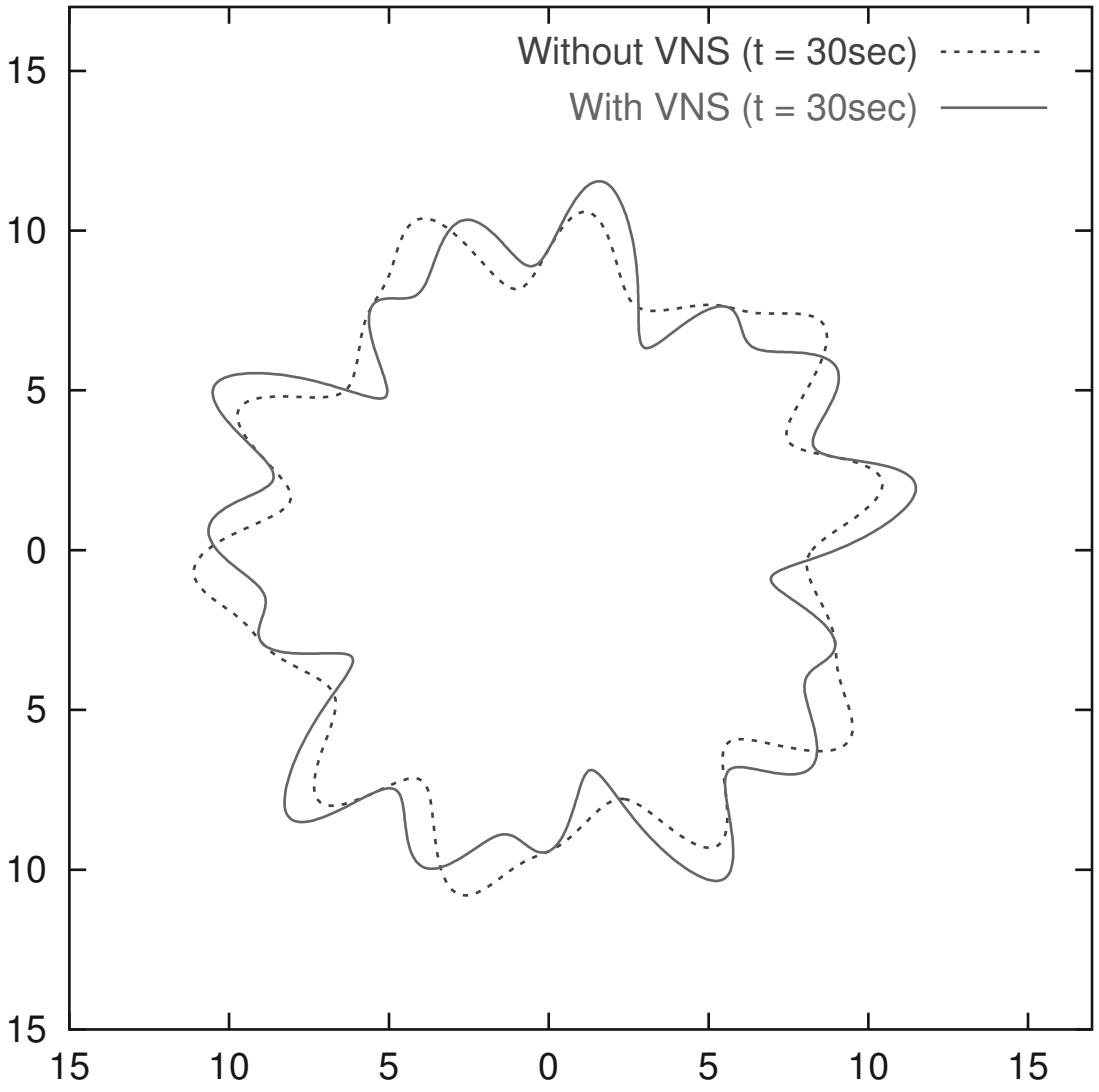

Figure 4.3: Comparison of the interfaces at $t = 30\,\text{sec}$ with and without VNS

interface seem to coincide with the nonlinear features of the fingering phenomena pointed by Homsy in [26], which consist of the repetitive processes of fingers' tip-spreading and splitting.

Figures 4.4 and 4.5 also show the nonlinear evolution without VNS and with VNS, respectively. In these cases, the modes n are chosen as $n = 6$, 12, 18, which is different from those of Figs. 4.1 and 4.2. All the parameters and the initial conditions are the same, while the difference of mode n causes the difference of the number of the fingers. The time intervals of curves in Figs. 4.4 and 4.5 correspond to those in Figs. 4.1 and 4.2. Similarly to the Figs. 4.1 and 4.2, one can convince again that the interface becomes more unstable and the tip splitting occurs more often in the case of taking VNS into consideration. This can be seen by comparing the interfaces with and without VNS at $t = 30\,\mathrm{sec}$, as depicted in Fig. 4.6.

As shown in Figs. 4.3 and 4.6, the perturbed interface becomes more unstable and perturbation amplitude has a large value when the VNS effect is taken into consideration. Analytically, such differences are caused by the strength of the coupling between the main mode n and the other modes n', appeared in $\Gamma(n, n')$ defined by (4.2.5). Our analysis with VNS corresponds to the case of nonzero ϵ in (4.2.5), while the previous analysis neglecting VNS is equivalent to the case $\epsilon = 0$. This indicates that the effect of VNS increases the value of the nonlinear term $\Xi(n, t)$ in the extended mode coupling equation (4.3.5). The larger value of $\Xi(n, t)$ leads to the larger deviation of $\zeta_n(t)$ from $\zeta_n^{lin}(t)$ in (4.3.7) than that without VNS.

Hence we may conclude that VNS definitely affects the nonlinear behaviour of the radially growing interface, and therefore it should not be neglected.

4.4 Conclusions

In this chapter we focused on the effects of VNS upon a radial growth of the interface in a Hele-Shaw cell. As mentioned in the previous section, VNS is defined by viscosity and the velocity gradient, so that it may affect instability of a radially growing, and deforming interface. Under such a background, we employed the normal stress balance (4.1.1) due to [57] as one of the boundary conditions, instead of the traditional Young–Laplace equation. Then, in Section 4.2 we derived the extended mode coupling equation (4.2.3) up to the second order in the perturbation amplitudes $\zeta_n(t)$, which includes the VNS effects in the complete form. We emphasize that the extended mode coupling equation (4.2.3) is a generalized one compared with those in [44, 57, 58]. When we neglect the nonlinear term, the extended mode coupling equation (4.2.3) and the linear growth rate (4.2.4) are the same as (17) and (18) in [57], respectively.

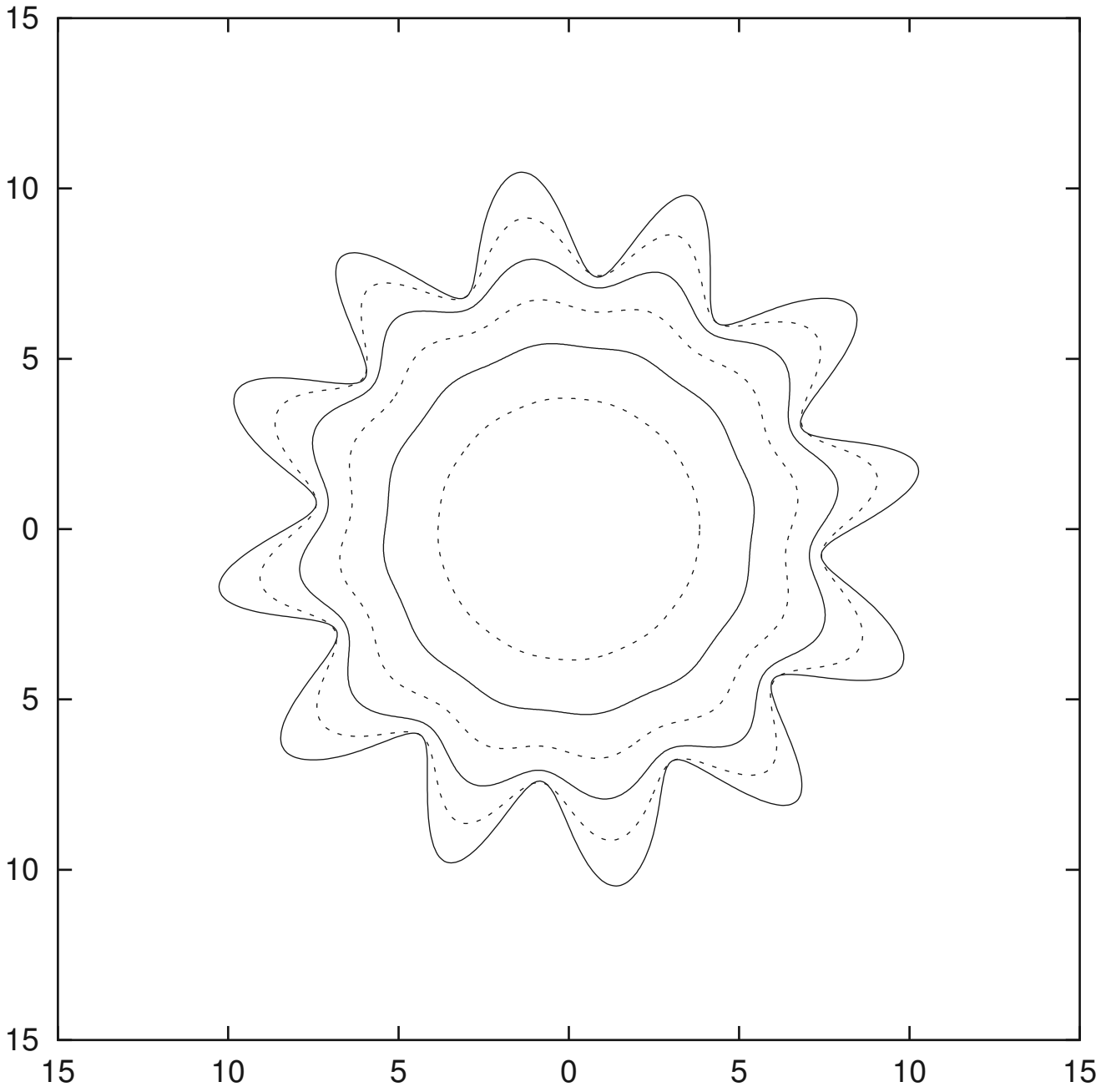

Figure 4.4: Interface growth without VNS from $t = 5$ to 30 sec. The modes are chosen as $n = 6$, 12, 18.

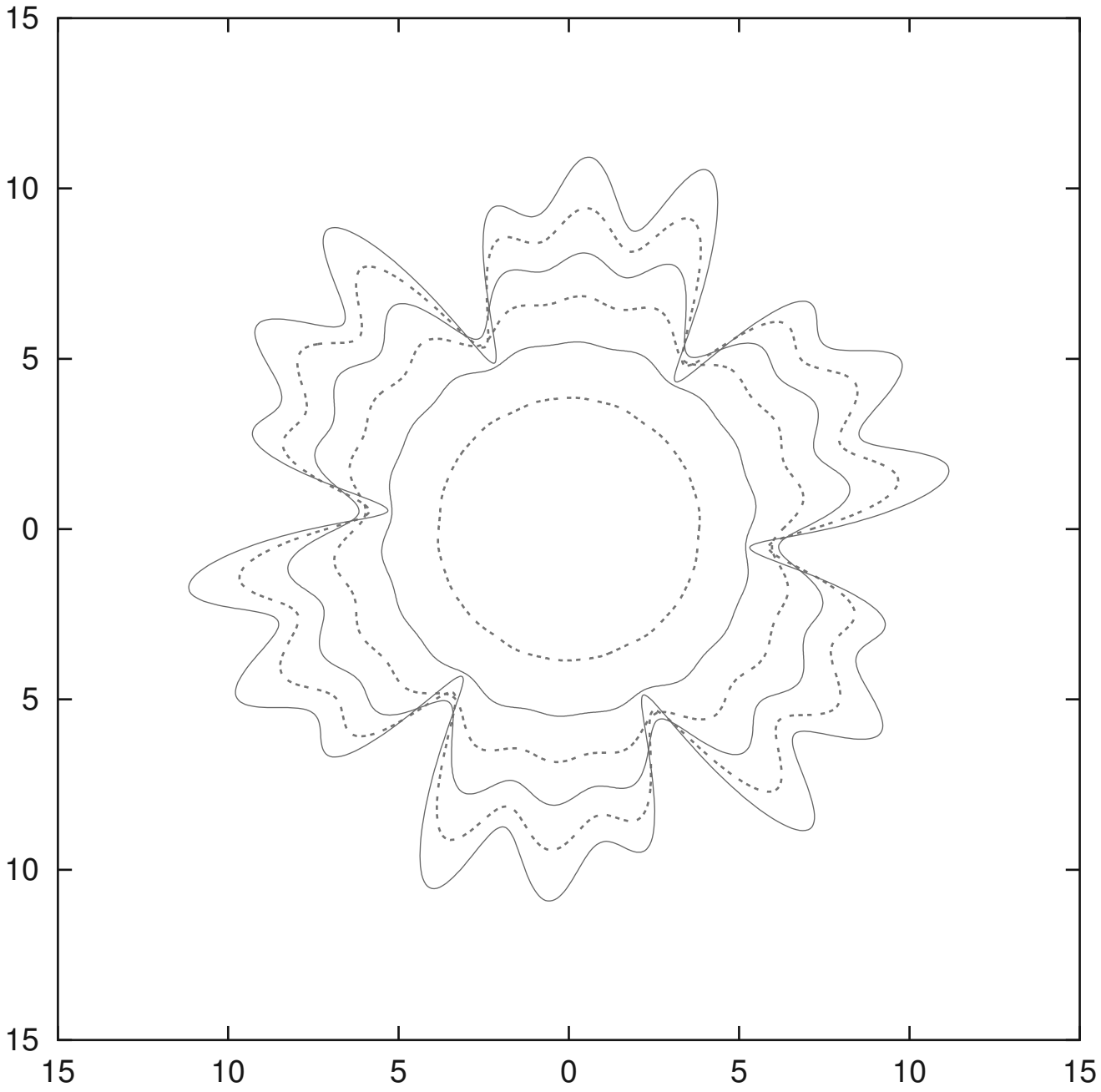

Figure 4.5: Interface growth with VNS from $t = 5$ to 30 sec. The modes are chosen as $n =$ 6, 12, 18.

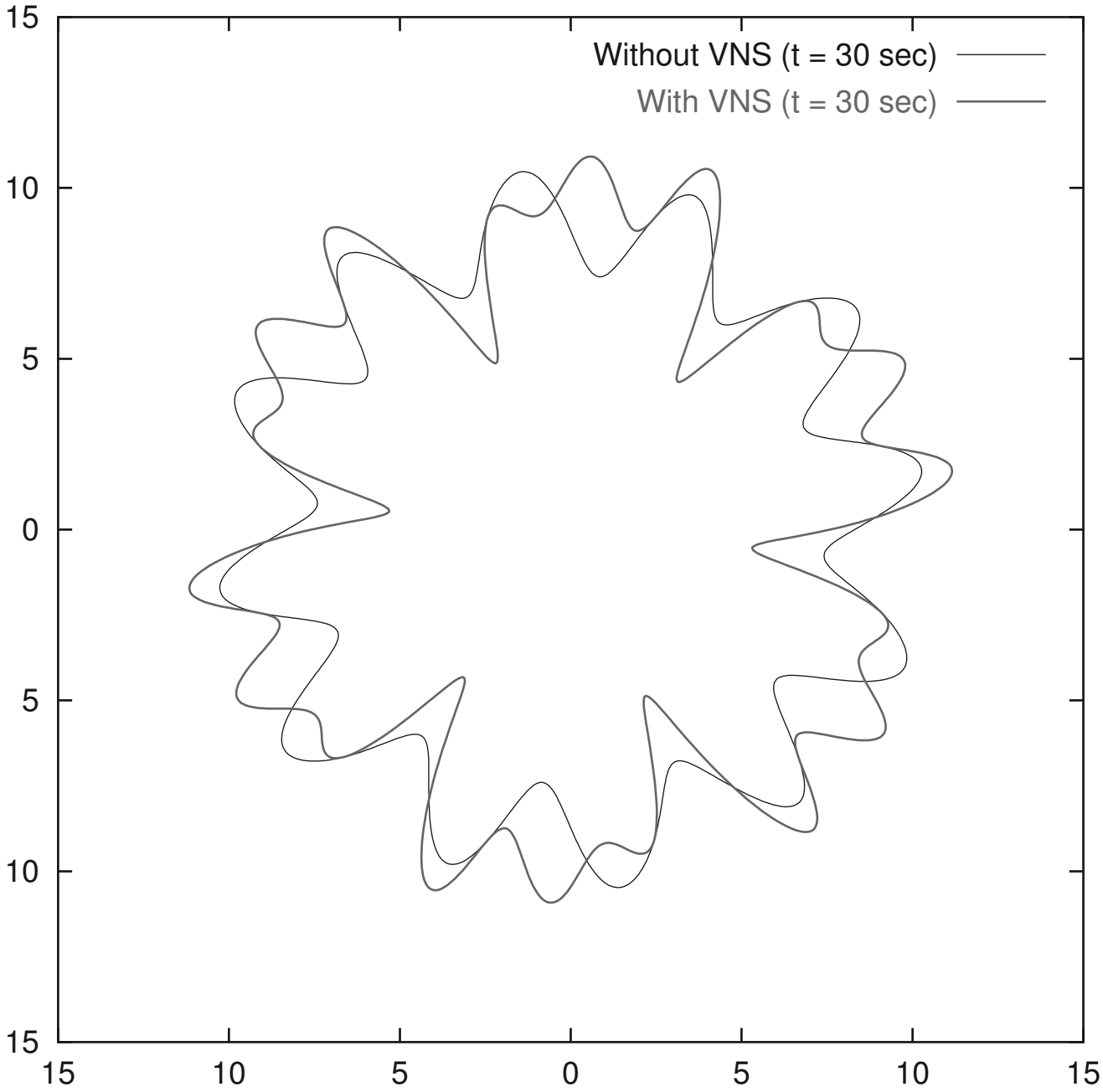

Figure 4.6: Comparison of the interfaces at $t = 30\,\text{sec}$ with and without VNS.

Similarly, it can be easily shown that the extended mode coupling equation (4.2.3) is the same as Eq. (18) in [44] for the case of $\epsilon = 0$, *i.e.*, neglecting the VNS terms.

Following the analysis in [44, 58], we numerically calculated the time evolution of the weakly nonlinear interfaces with and without VNS as depicted in Figs. 4.1-4.6. The differences between the interfaces with and without VNS at the same time are shown in Figs. 4.3 and 4.6. Judging from these figures, nonlinear features of the viscous fingering such as tip-spreading and splitting can be seen in the case of considering the effect of VNS. These suggest that VNS certainly affects the instability on a radially growing interface and it seems to be more appropriate to take VNS into consideration.

Therefore, we can conclude that VNS significantly affects such nonlinear features on the radial fingering phenomena. Finally, we emphasize that the VNS effect should be included in a lot of models which have been considered by Young–Laplace equation.

Chapter 5

Weakly Nonlinear Analysis with the Effect of Wetting Layer in Hele-Shaw Cell

In this chapter we introduce another appropriate boundary condition, which contains the effect of wetting layer in Hele-Shaw cells. As mentioned in Chapter 4, it has been doubted whether Young–Laplace equation (3.2.11) is valid or not, especially, when the effect of surface tension is not negligible. McLean and Saffman pointed out that the discrepancies between theoretical and experimental results are caused by Young–Laplace equation, and proposed the expected form of the boundary condition in [14]. Subsequently, Park and Homsy obtained an improved boundary condition explicitly [15]. As will be explained in the next section, their boundary condition includes the wetting layer effect of displaced fluid. Employing their boundary condition, we derive an extended mode coupling equation and carry out weakly nonlinear analysis.

5.1 Boundary Condition including the Effect of Wetting Layer

By following the work due to McLean and Saffman, Park and Homsy focused on the thin wetting film of the displaced fluid adherent to a Hele-Shaw cell, as shown in Fig. 5.1. In [15], they derived the boundary condition by dividing the interface into three regions: the

clear-original-fluid region (Region I), the capillary-static region (Region II), and the constant-film-thickness region (Region III), as shown in Fig. 5.1. Then they accomplished an asymptotic analysis to correct the Young–Laplace equation in terms of the power of the capillary number Ca.

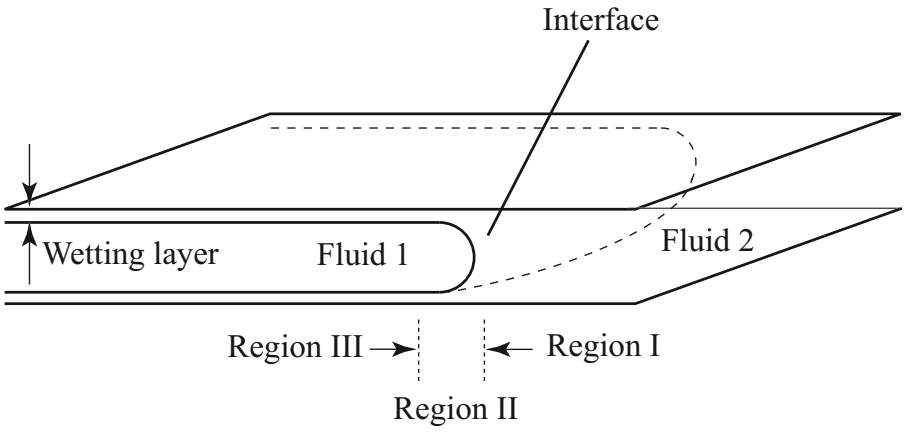

Figure 5.1: The wetting layer on the cell and three regions

The boundary condition proposed by Park and Homsy [15] is

$$p_1 - p_2 = \sigma \left[\frac{2}{b} + \frac{\pi}{4} H \right] + \frac{2\sigma J}{b} Ca^{2/3}, \tag{5.1.1}$$

where $J = 3.8$, H is the two-dimensional curvature of the plane parallel to the cell, and σ is the surface-tension coefficient. Moreover, $Ca = \mu_2 U/\sigma$ is the capillary number with U being the characteristic velocity determined by Darcy's law as

$$U = \frac{b^2}{12\mu_2} \nabla\phi_2 \cdot \mathbf{n}. \tag{5.1.2}$$

The first and second terms on the right hand side in (5.1.1) is caused by a capillary static effect. It should be noted that the coefficient $\pi/4$ in the second term is different from that in the Young–Laplace equation

$$p_1 - p_2 = \sigma \left(\frac{2}{b} + H \right). \tag{3.2.11}$$

In Eq. (5.1.1), the third term comes from the effect of moving meniscus at the interface, which is negligible if the flow is sufficiently slow.

The applicability of this boundary condition (5.1.1) is verified in accordance with the experimental results for the case of radial geometry, for instance, in [20]. There, it was shown that

the relationship between capillary number Ca and the most unstable wavelength of the growing interface; the relationship was improved by employing the boundary condition (5.1.1), compared with those by using the Young–Laplace equation (3.2.11). These results are considered enough to indicate the validity of the new boundary condition (5.1.1).

Although this boundary condition has been employed in numerous theoretical and experimental works to improve the previous results obtained by applying the Young–Laplace equation [16, 20, 62], it has never been applied to radial geometry, except in a study by Martyushev and Birzina [63]. They carried out a linear analysis and clarified the relationship between the radius of the interface $R(t)$ and that of the cell R_∞. However, they did not investigate how the wetting layer affects the interface patterns.

Accordingly, it should be necessary to carry out a nonlinear analysis based on the boundary condition (5.1.1) that takes the wetting effect into consideration. Therefore the objectives of this chapter are as follows: (i) to carry out a weakly nonlinear analysis on the perturbation of the interface under the boundary condition (5.1.1), and (ii) to visualize the time evolution of the perturbed interfaces with and without the wetting effect (see also [64]).

It is significant to compare the results obtained by boundary condition including the wetting effect with those by boundary condition including the VNS effect.

5.2 Derivation of the Mode Coupling Equation

In this section, the mode coupling equation is derived under the boundary condition proposed by Park and Homsy [15]. The derivation is similar to that shown in Chapter 3, by following [44]. By substituting the general solution ϕ_i (3.3.3) and (3.3.4) and perturbation ζ into the kinematic boundary condition (3.3.8) and the boundary condition (5.1.1), and then eliminating ϕ_{in}, the following mode coupling equation can be obtained:

$$\dot{\zeta}_n = \Lambda(n)\zeta_n + \sum_{n' \neq 0} \Gamma(n, n')\zeta_{n'}\zeta_{n-n'}, \tag{5.2.1}$$

where

$$\Lambda(n) = \frac{Q}{2\pi R^2}(A|n|-1) - \frac{\pi}{4}\frac{\alpha}{R^3}|n|(n^2-1) - \epsilon\frac{J'\alpha}{b^{5/3}\sigma^{2/3}}\left(\frac{Q}{2\pi R}\right)^{2/3}|n|(A|n|-1), \quad (5.2.2)$$

$$\begin{aligned}\Gamma(n,n') = {} & \frac{1}{R}\left[\frac{Q}{2\pi R^2}\left(A|n|\left\{A|n'|(1-\mathrm{sgn}(nn'))-\frac{1}{2}\right\}-(A|n'|-1)\right)\right. \\ & \left.-\frac{\pi}{4}\frac{\alpha}{R^3}\left(|n|\left(1-\frac{1}{2}nn'-\frac{3}{2}n'^2\right)+\{A|n|(1-\mathrm{sgn}(nn'))-1\}|n'|(n'^2-1)\right)\right] \\ & -\epsilon\frac{|n|}{R}\frac{J'\alpha}{(b\sigma)^{2/3}}\left(\frac{Q}{2\pi R}\right)^{2/3}\left[A|n||n'|(\mathrm{sgn}(nn')-1)+\frac{A|n|}{b}\left(\frac{1}{2}-\mathrm{sgn}(nn')\right)+\frac{A}{2}|n'|-\frac{11}{6}\right. \\ & -\frac{1}{2}\left(3A-1-\frac{1}{|n'|}\right)n'(n-n')-\frac{1}{3R^2}(2A|n'|-5+3A|n-n'|(A|n'|-1)) \\ & +\frac{1}{b}(A|n'|-1)(|n|+|n'|)\left(A(1-\mathrm{sgn}(nn'))-\frac{1}{|n|}\right) \\ & \left.+\frac{2\pi}{Q}\frac{\pi}{4}\frac{\alpha}{R^3}\left\{|n'|(n'^2-1)(A|n-n'|-1)+(A|n'|-1)|n-n'|\left((n-n')^2-1\right)\right\}\right]. \end{aligned} \quad (5.2.3)$$

Here, $J' = (3.8\cdot 4)/(3\cdot 12^{1/3})$ and $\epsilon = \epsilon(t) = b^2/12R(t)^2$ is the thickness parameter of the cell. Note that ϵ is dependent on t and is effective during the early stages of the interface growth. In addition, $A = (\mu_2-\mu_1)/(\mu_2+\mu_1)$ is the viscosity contrast and $\alpha = b^2\sigma/12(\mu_1+\mu_2)$. Equation (5.2.1) is similar to the equation derived by Miranda and Widom [44] when ϵ is equal to zero. Moreover, the analytic results by Martyushev and Birzina [63] are identical to our results when $\Gamma(n,n') = 0$; therefore our analysis for the mode coupling equation (5.2.1) can be considered as an extension of those of Martyushev and Birzina.

5.3 Analysis of the Extended Mode Coupling Equation

5.3.1 Linear Approximated Solution

In this section, we seek for a solution of the mode coupling equation (5.2.1) derived above. First, by following [44], the linear equation can be solved as

$$\dot{\zeta}_n = \Lambda(n)\zeta_n, \quad (5.3.1)$$

which is obtained by neglecting the coupling term in equation (5.2.1). Equation (5.3.1) can be easily solved as

$$\zeta_n(t) = \zeta_n(0) \exp\left(\int_0^t \Lambda(n)\mathrm{d}t\right). \tag{5.3.2}$$

If $\Lambda(n) > 0$, the solution increases as t increases, which means the interface is unstable. Otherwise, if $\Lambda(n) < 0$, the solution decays, which corresponds to a stable interface. The condition $\Lambda(n) = 0$ leads to the critical radius $R_c = R_c(n)$ which is a root of

$$\left(R - \frac{\pi^2\alpha}{2Q}\frac{|n|(n^2-1)}{A|n|-1}\right)^3 = \frac{2\pi b}{Q}\left(\frac{J'\alpha|n|}{12\sigma^{2/3}}\right)^3 R.$$

Therefore, $\Lambda(n) > 0$ is equivalent to $R_c(n) > R(t)$; that is, the instability of the interface is determined by the magnitude relationship of $R(t)$ and $R_c(n)$. By following the analysis due to Miranda and Widom [44], the linear approximated solution of the linear equation (5.3.1) can be obtained as

$$\zeta_n^{\mathrm{lin}}(t) = \begin{cases} \zeta_n(0) & (R(t) < R_c), \\ \zeta_n(0)\left(\dfrac{R}{R_c}\right)^{A|n|-1} \exp\left[(A|n|-1)\left(\dfrac{R_c}{R} - 1\right)\right] & \\ & (R(t) > R_c). \end{cases} \tag{5.3.3}$$

Note that the form of this solution (5.3.3) is identical to the form obtained by Miranda and Widom; however, the definition of $R_c(n)$ itself is different from theirs.

5.3.2 Nonlinear Approximated Solution

In this section, we derive the nonlinear approximated solution of the mode coupling equation (5.2.1). By applying the method used by Miranda and Widom [44] again, the following mode coupling equation, whose coupling term $\zeta_{n'}\zeta_{n-n'}$ is replaced by $\zeta_{n'}^{\mathrm{lin}}\zeta_{n-n'}^{\mathrm{lin}}$, is obtained:

$$\dot{\zeta_n} = \Lambda(n)\zeta_n + \Xi(n,t), \tag{5.3.4}$$

$$\Xi(n,t) = \sum_{n'\neq 0} \Gamma(n,n')\zeta_{n'}^{\mathrm{lin}}(t)\zeta_{n-n'}^{\mathrm{lin}}(t). \tag{5.3.5}$$

Here, $\Lambda(n)$ and $\Gamma(n,n')$ are defined as (5.2.2) and (5.2.3), respectively. Then, the nonlinear approximated solution of the equation (5.3.4) can be expressed by the linear equation (5.3.3)

as follows:

$$\zeta_n(t) = \begin{cases} \zeta_n(0) & (R(t) < R_c), \\ \zeta_n^{\mathrm{lin}}(t)\left\{1 + \displaystyle\int_{t_c(n)}^{t} \frac{\Xi(n,t')}{\zeta_n^{\mathrm{lin}}(t')}\mathrm{d}t'\right\} & \\ & (R(t) > R_c), \end{cases} \tag{5.3.6}$$

where $t_c(n)$ is the critical time defined by $R(t_c(n)) = R_c(n)$. If $Ca = 0$ in $\Gamma(n, n')$, the solution (5.3.6) corresponds to the one obtained by Miranda and Widom [44]. Therefore, our solution (5.3.6) is an extension of their solutions. Based on this nonlinear approximated solution (5.3.6), we can numerically calculate the time evolution and thereby visualize the behaviour of the perturbed interface $\mathcal{R} = R(t) + \zeta(\theta, t)$ from $t = 3$ to 18 sec, as depicted in Figs. 5.2 (without the wetting effect) and 5.3 (with the wetting effect). The parameters are chosen as $b = 0.15$ cm, $Q = 9.3\,\mathrm{cm}^3/\mathrm{s}$, $\sigma = 63$ dynes/cm, and $R_0 = 0.05$ cm, which are the same as those used in Paterson's experiments [19]. The amplitude of the initial perturbation is $R_0/500$, and the modes of the perturbation are set to $n = 4, 8$, and 12. Here these modes are chosen in order to reveal the effect of wetting layer on the nonlinear features of viscous fingering such as finger tip-splitting. However it is to be noted that the modes other than $n = 4, 8$, and 12 can be included in the phenomena. It is necessary to examine which mode will be dominant among the all possible modes.

In both figures, the time interval of each curve is 5 sec. Without the wetting effect, the interface remains circular, except at $t = 18$ sec, which the circle is only slightly unstable as shown in Fig. 5.2. In contrast, the appearance is quite different for the case in which the wetting effect is included. The interface remains stable during the earlier stages of growth, and gradually becomes unstable (at $t = 13$ sec). Eventually, each tips of the four-fold fingers are split into three (at $t = 18$ sec), as seen in Fig. 5.3. This tip-splitting of fingers, which is often observed in such experiments, is considered to be one of the typical nonlinear features of viscous fingering [19]. Figures 5.2 and 5.3 suggest that the nonlinear features are caused by the wetting effect. In other words, we can conclude that our model reflects the nonlinear behaviour of the interface effectively.

Finally, Fig. 5.4 shows the time evolution of the interface including the VNS effect under the same initial condition used in Figs. 5.2 and 5.3 (see also numerical results by the author [64]). Comparing Fig. 5.4 with Figs. 5.2 and 5.3, we found that the effect of wetting layer enhances the instability more than that of VNS. The splitting of the fingers is seen in Fig. 5.3 at 18 sec,

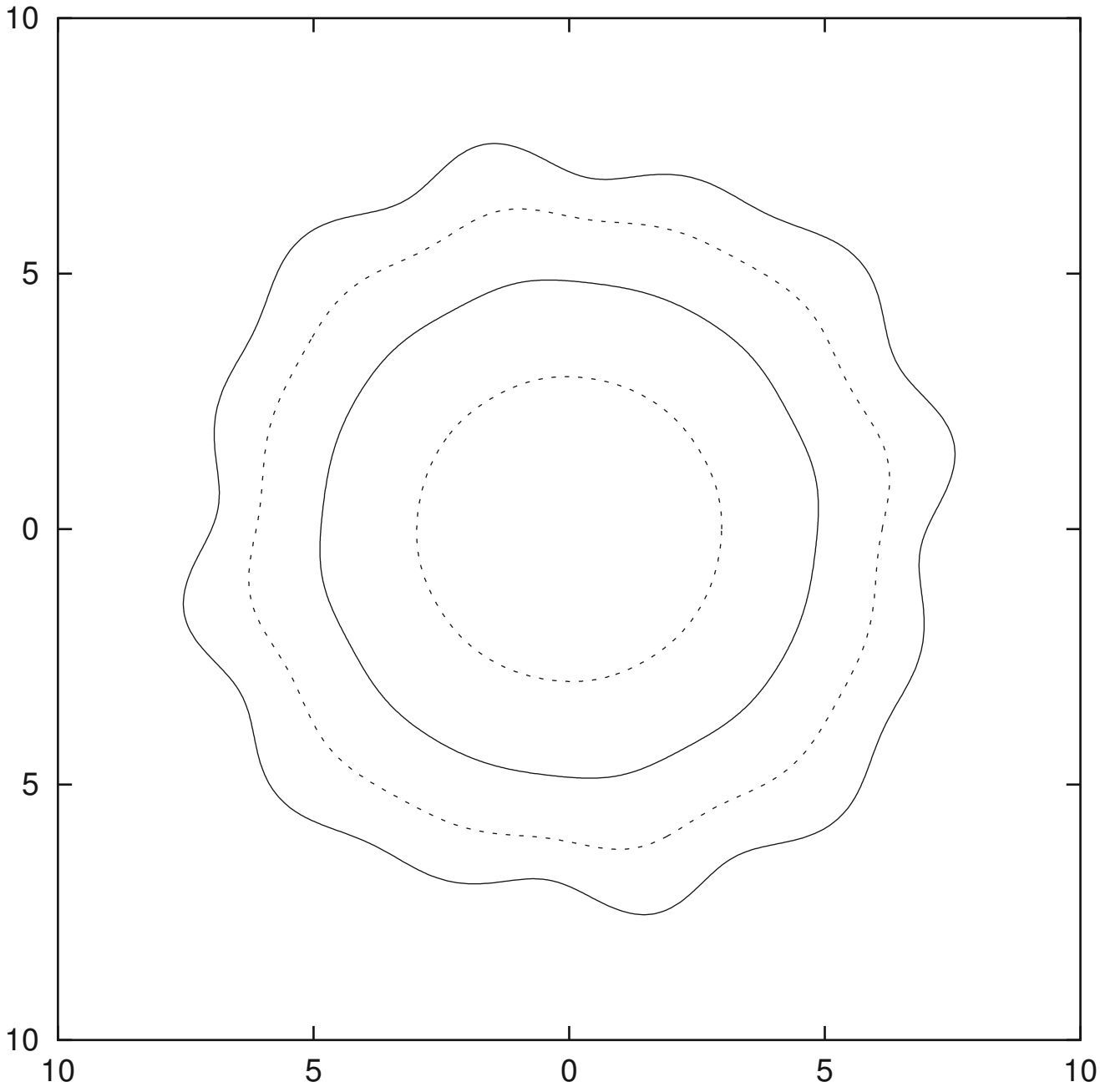

Figure 5.2: Time evolution of the interface without the wetting effect, from $t = 3$ to 18 sec. The modes are chosen as $n = 4$, 8, 12.

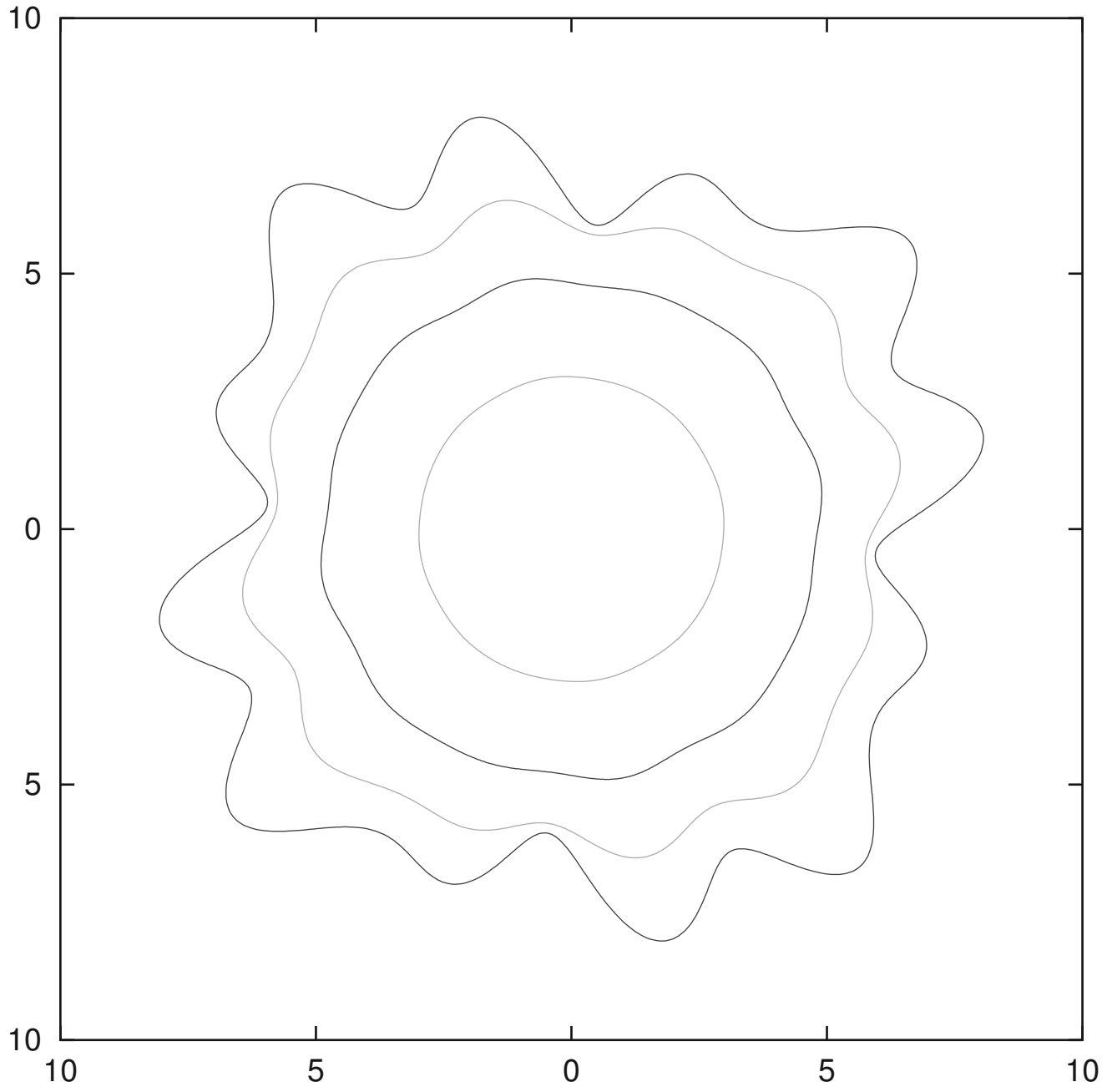

Figure 5.3: Time evolution of the interface with the wetting effect, from $t = 3$ to 18 sec. The modes are chosen as $n = 4$, 8, 12.

while it is not yet clearly seen in Fig. 5.4.

5.4 Conclusions

In this study, we investigate the Hele-Shaw problem with a boundary condition which includes the effect of the wetting layer of a displaced fluid. This boundary condition was originally proposed by Park and Homsy in their pioneering work [15], for the rectangular geometry; they also carried out a linear analysis of the interface. Although the boundary conditions for the Hele-Shaw problem are still controversial [62], the effect of the wetting layer on the fingering patterns has not been investigated.

In this chapter, we focused on the pattern formation of the interface and accomplish a weakly nonlinear analysis under the effect of the wetting layer. In order to clarify how the time evolution of the interface is affected by the wetting effect, a mode coupling equation was derived from the boundary condition. The mode coupling equation derived by Miranda and Widom [44] is based on the Young–Laplace equation, which is valid for the rigid motion of an interface without any deformation. In contrast to the one by employing Young–Laplace equation, our mode coupling equation reflects the deformation of the interface effectively, and therefore our equation is considered to be an actual extension of the equation derived by Miranda and Widom [44]. Moreover, the numerical results shown in Figs. 5.2 and 5.3 support the tip-splitting of the fingers for the case that the wetting effect works, which is one of the typical nonlinear features of viscous fingering phenomena. Consequently, these facts imply that the effect of the wetting layer in the cell plays a significant role on the nonlinear behaviour of an unstable interface.

Finally, it should be noted that we do not have any criteria so far to conclude which boundary condition is more appropriate.This will be done by comparing the present results with the experiments in future work.

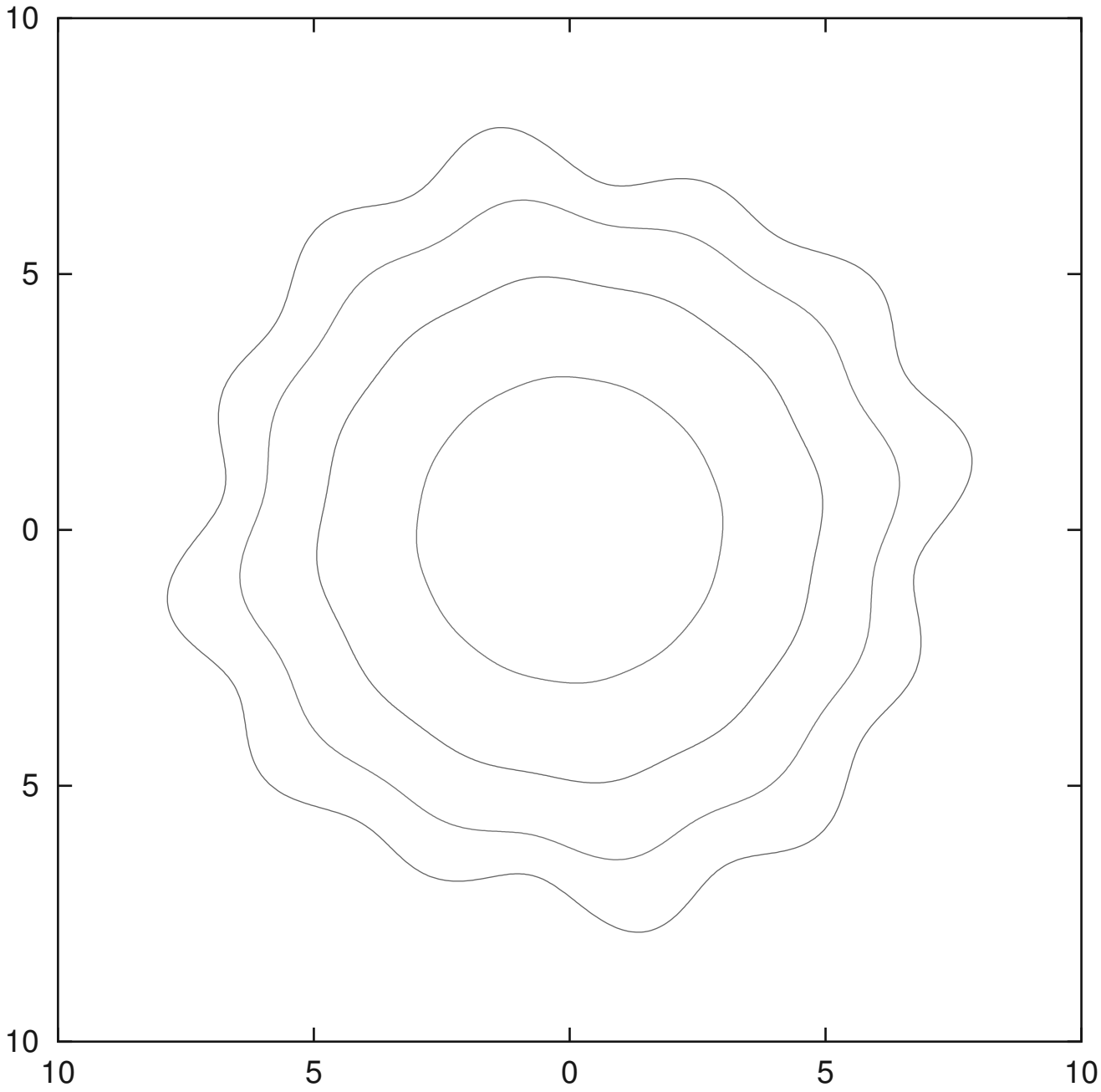

Figure 5.4: Time evolution of the interface with the VNS effect, from $t = 3$ to 18 sec. The modes are chosen as $n = 4$, 8, 12.

Chapter 6

Concluding Remarks

In this Thesis, we investigate the effect of boundary condition for the Hele-Shaw problem. The validity of Young–Laplace equation has been doubted for ages, because of some qualitative difference between the theoretical and experimental results. In addition to this, Young–Laplace equation is derived on the postulate that the interface is static, or translates rigidly without any deformation. These facts require us to seek for the more appropriate boundary conditions.

The boundary condition which take VNS terms into account is naturally followed from the normal stress balance at the interface. Then mode coupling equation including this VNS effect is derived. In Chapter 4 it was confirmed that VNS terms clearly affect the instability of the interface; the interface tends to become more unstable than that for the case of Young–Laplace equation. Moreover, the nonlinear features of viscous fingering, such as tip splitting, can be seen in the numerical results. From these results, it is concluded that the boundary condition with VNS is more realistic for interpretation of experiments than the Young–Laplace equation.

Next, another boundary condition with the wetting layer effect is considered. In similar to the boundary condition with VNS, the mode coupling equation is derived. In Chapter 5, results similar to those in Chapter 4 were obtained by weakly nonlinear analysis, which suggest that the interface is more unstable than the one obtained by Young–Laplace equation. Numerical results show the nonlinear features, as seen in Chapter 4 as well. Thus, the boundary condition including the effect of wetting layer is considered to be more appropriate than Young–Laplace equation for considering the experiments.

However, so far it is difficult to conclude which boundary condition, with VNS or wetting effect describes fingering phenomena more appropriately. Based on the present study, we expect the difference between the time dependence of the effect of VNS and the effect of wetting layer.

It will be examined by experimental observations.

There remains a lot of open problems to study in the morphologies of growing interfaces in Hele-Shaw cells.

Appendix

Proof of the convection theorem

Convection theorem

If Ω_t is a fluid domain in E^3, and if $f(\boldsymbol{x}, t) \in C^1(\bar{\Omega}_t)$, then

$$\frac{\mathrm{d}}{\mathrm{d}t}\int_{\Omega_t} f \,\mathrm{d}V = \int_{\Omega_t} \left(\frac{\mathrm{D}f}{\mathrm{D}t} + f\,\nabla\cdot\boldsymbol{v}\right)\mathrm{d}V, \tag{A.1}$$

where $\mathrm{d}V$ denotes the volume element.

Corollary 2.1.1

For Ω_t and f as in the convection theorem, let $\Omega_1 = \Omega_{t_1}$ at any fixed t_1 with a regular boundary $\partial\Omega_1$. Then

$$\frac{\mathrm{d}}{\mathrm{d}t}\int_{\Omega_t} f \,\mathrm{d}V\bigg|_{t=t_1} = \frac{\partial}{\partial t}\int_{\Omega_1} f \,\mathrm{d}V + \int_{\partial\Omega_1} f\,\boldsymbol{v}\cdot\mathbf{n}\,\mathrm{d}S$$

holds, where $\mathbf{n}$ is the unit outward normal to $\partial\Omega_1$, and $\mathrm{d}S$ is the surface element on $\partial\Omega_1$.

Proof

From postulating $\Omega_t = H_t\Omega_0$ with Ω_0 being a bounded fixed reference domain, it follows that

$$\int_{\Omega_t} f \,\mathrm{d}V = \int_{\Omega_0} g(\boldsymbol{a}, t)\,\mathbf{J}(\boldsymbol{a}, t)\,\mathrm{d}V_0,$$

where $\boldsymbol{a}$ is the Lagrangian coordinates which represent the position of a fluid particle at $t = 0$, *i.e.*, $\boldsymbol{a} \in \Omega_0$. In the above, $f(\boldsymbol{x}, t) = g(\boldsymbol{a}, t)$, $\boldsymbol{x} = x(\boldsymbol{a}, t) \in \Omega_t$ and $\mathbf{J} = \det\left(\partial x_i/\partial a_k\right)$ is the

Jacobian determinant. Thus

$$\begin{aligned}\frac{\mathrm{d}}{\mathrm{d}t}\int_{\Omega_t} f\,\mathrm{d}V &= \frac{\partial}{\partial t}\int_{\Omega_0} g(\boldsymbol{a},t)\,\mathbf{J}(\boldsymbol{a},t)\,\mathrm{d}V_0 \\ &= \int_{\Omega_0}\frac{\partial}{\partial t}(g(\boldsymbol{a},t)\,\mathbf{J}(\boldsymbol{a},t))\;\mathrm{d}V_0,\end{aligned}$$

since $\partial(g\mathbf{J})/\partial t$ is continuous. Since

$$\frac{\partial(g\mathbf{J})}{\partial t} = \mathbf{J}\,\frac{\mathrm{D}f}{\mathrm{D}t} + f\,\frac{\partial\mathbf{J}}{\partial t},$$

and it is easily shown that $\partial\mathbf{J}/\partial t = \mathbf{J}\mathrm{div}\,\boldsymbol{v}$, then

$$\begin{aligned}\frac{\mathrm{d}}{\mathrm{d}t}\int_{\Omega_t} f\,\mathrm{d}V &= \int_{\Omega_0}\frac{\partial}{\partial t}(g(\boldsymbol{a},t)\,\mathbf{J}(\boldsymbol{a},t))\;\mathrm{d}V_0 \\ &= \int_{\Omega_0}\left(\mathbf{J}\,\frac{\mathrm{D}f}{\mathrm{D}t} + f\,\mathbf{J}\mathrm{div}\,\boldsymbol{v}\right)\mathrm{d}V_0,\end{aligned}$$

from which (A.1) follows.

Corollary (2.1.1) is proven from Convection theorem by noticing that

$$\frac{\mathrm{D}f}{\mathrm{D}t} + f\,\mathrm{div}\,\boldsymbol{v} = \frac{\partial f}{\partial t} + \mathrm{div}\,(f\boldsymbol{v}),$$

and that

$$\int_{\Omega_1}\mathrm{div}\,(f\boldsymbol{v})\,\mathrm{d}V = \int_{\partial\Omega_1}(f\,\boldsymbol{v})\cdot\mathbf{n}\,\mathrm{d}S$$

by the Divergence theorem.

Bibliography

[1] J. Kepler, The Six-Cornered Snowflake, 1611; translated by L. L. Whyte, Oxford Univ. Press (1966).

[2] U. Nakaya, M. Hanajima, J. Muguruma, Physical Investigations on the Growth of Snow Crystals, Journal of the Faculty of Science, Hokkaido University. Ser. 2, (1958) 87-118.

[3] T. Kobayashi, On the Variation of Ice Crystal Habit with Temperature, Physics of Snow and Ice, Part 1, ed. H. Oura, Inst. Low Temp. Sci., Hokkaido Univ., Sapporo (1967) 95.

[4] D. W. Thompson, On Growth and Form, (1917)

[5] P. Glansdorff, I. Prigogine, Thermodynamic theory of structure, stability and fluctuations, John Wiley and Sons, 1971.

[6] A. M. Turing, The Chemical Basis of Morphogenesis, Phil. Trans. Roy. Soc. London. B **237** (1952) 37-72.

[7] B. P. Belousov, A Periodic Reaction and Its Mechanism, Oscillations and traveling waves in chemical systems. Wiley, New York (1985).

[8] A. M. Zhabotinsky, Periodic Liquid Phase Reactions, Proc. Ac. Sci. USSR **157** (1964) 392-395.

[9] S. Kondo and R. Asai, A Reaction-Diffusion Wave on the Skin of the Marine Angelfish *Pomacanthus*, Nature **376** (1995) 765-768.

[10] J. Wakita, K. Komatsu, A. Nakahara, T. Matsuyama, M. Matsushita, Experimental Investigation on the Validity of Population Dynamics Approach to Bacterial Colony Formation, J. Phys. Soc. Jpn. **63** (1994) 1205-1211.

[11] 寺田寅彦，寺田寅彦随筆集，岩波書店 (1947).

[12] P. G. Saffman, G. I. Taylor, The Penetration of a Fluid into Porous Medium or Hele-Shaw Cell Containing a More Viscous Liquid, Proc. Roy. Soc. London A **245** (1958) 312-329.

[13] R. Chouke, P. van Meurs, C. van der Poel, The Instability of Slow, Immiscible, Viscous Liquid-Liquid Displacements in Permeable Media, Trans. AIME **216** (1959) 188-194.

[14] J. W. McLean, P. G. Saffman, The Effect of the Surface Tension on the Shape of Fingers in a Hele Shaw Cell, J. Fluid Mech. **102** (1981) 455-469.

[15] C. W. Park, G. M. Homsy, Two-Phase Displacement in Hele-Shaw Cells: Theory, J. Fluid Mech. **139** (1984) 291-308.

[16] L. Schwartz, Stability of Hele-Shaw Flows: The Wettinglayer Effect, Phys. Fluids **29** (1986) 3086-3088.

[17] P. Tabeling, G. Zocchi and A. Libchaber, An Experimental Study of the Saffman–Taylor Instability, J. Fluid. Mech. **177** (1987) 67-82.

[18] J. Bataille, Stabilité d'un écoulement Radial non Miscible, Revue Inst. Pétrole, **23** (1968) 1349.

[19] L. Paterson, Radial Fingering in a Hele Shaw Cell, J. Fluid Mech. **113** (1981) 513-529.

[20] T. Maxworthy, Experimental Study of Interface Instability in a Hele-Shaw Cell, Phys. Rev. A **39** (1989) 5863-5866.

[21] H. Thomé, M. Rabaud, V. Hakim, Y. Couder, The Saffman–Taylor Instability: From the Linear to the Circular Geometry, Phys. Fluids A **1** (1989) 224-240.

[22] A. Leshchiner, M. Thrasher, M. Mineev-Weinstein, H. Swinney, Harmonic Moment Dynamics in Laplacian Growth, Phys. Rev. E **81** (2010) 016206.

[23] G. I. Taylor, The Instability of Liquid Surfaces when Accelerated in a Direction Perpendicular to their Planes. I, Proc. Roy. Soc. London. A **201** (1950) 192-196.

[24] D. J. Lewis, The Instability of Liquid Surfaces when Accelerated in a Direction Perpendicular to their Planes. II, Proc. Roy. Soc. London. A **202** (1950) 81-96.

[25] H. S. Hele-Shaw, Flow of Water, Nature **58** (1898) 34.

[26] G. M. Homsy, Viscous Fingering in Porous Media, Ann. Rev. Fluid Mech. **19** (1987) 271-311.

[27] S. D. Howison, Fingering in Hele-Shaw Cell, J. Fluid Mech. **167** (1986) 439-453.

[28] P. G. Saffman, Viscous Fingering in Hele-Shaw Cells, J. Fluid Mech. **173** (1986) 73-94.

[29] S. Tanveer, The effect of surface tension on the shape of a Hele-Shaw cell bubble, Phys. Fluids **29** (1986) 3537.

[30] D. A. Reinelt, The Rate at Which a Long Bubble Rises in a Vertical Tube, J. Fluid Mech. **175** (1987) 557-565.

[31] R. M. Davies, G. I. Taylor, The Mechanics of Large Bubbles Rising Through Extended Liquids and Through Liquids in Tubes, Proc. Roy. Soc. London. A **200** (1950) 375-390.

[32] P. Ya. Polubarinova-Kochina, On a Problem of the Motion of the Contour of a Petroleum Shell, Dokl. Akad. Nauk USSR, **47** (1945) 254-257.

[33] L. A. Galin, Unsteady Filtration with a Free Surface, Dokl. Akad. Nauk USSR, **47** (1945) 246-249.

[34] B. Gustafsson, A. Vasil'ev, Conformal and Potential Analysis in Hele-Shaw Cells, Birkhäuser (2006).

[35] S. Richardson, Hele Shaw Flows with a Free Boundary Produced by the Injection of Fluid into a Narrow Channel, J. Fluid. Mech. **56** (1972) 609-618.

[36] E. Ben-Jacob, R. Godbey, N. D. Goldenfeld, J. Koplik, H. Levine, T. Mueller, L. M. Sander, Experimental Demonstration of the Role of Anisotropy in Interfacial Pattern Formation, Phys. Rev. Lett **55** (1985) 1315-1318.

[37] D. A. Kessler, J. Koplik, H. Levine, Pattern Selection in Fingered Growth Phenomena, Adv. Phys. **37** (1988) 255-339.

[38] J.-D. Chen, Radial viscous fingering patterns in Hele-Shaw cells, Experiments in Fluids **5** (1987) 363-371.

[39] M. Ohgiwari, M. Matsushita, T. Matsuyama, Morphological Changes in Growth Phenomena of Bacterial Colony Patterns, J. Phys. Soc. Jpn. **61** (1992) 816-822.

[40] K. Nakayama, H. Segur, M. Wadati, Integrability and the Motion of Curves, Phys. Rev. Lett. **69** (1992) 2603-2606.

[41] M. Mineev-Weinstein, P. B. Wiegmann, A. Zabrodin, Integrable Structure of Interface Dynamics, Phys. Rev. Lett. **84** (2000) 5106-5109.

[42] O. Agam, E. Bettelheim, P. B. Wiegmann, A. Zabrodin, Viscous Fingering and the Shape of an Electronic Droplet in the Quantum Hall Regime, Phys. Rev. Lett. **88** (2002) 236801.

[43] P. Pelcé, Dynamics of Curved Fronts, Academic Press (1988).

[44] J. A. Miranda, M. Widom, Radial Fingering in a Hele-Shaw Cell: A Weakly Nonlinear Analysis, Physica D **120** (1998) 315-328.

[45] G. Batchelor, An Introduction to Fluid Dynamics, Cambridge University Press (2000).

[46] E. C. Bingham, An Investigation of the Laws of Plastic Flow, U.S. Bureau of Standards Bulletin, **13** (1916) 309-353.

[47] 中村喜代次, 非ニュートン流体力学, コロナ社 (1997).

[48] R. Meyer, Introduction to Mathematical Fluid Dynamics, Dover publications (1971).

[49] 棚橋隆彦, 物質の構成方程式 (連続体の力学:3) 理工図書 (1986).

[50] K. R. Rajagopal, A new development and interpretation of the Navier-Stokes fluid which reveals why the "Stokes assumption" is inapt, International Journal of Non-Linear Mechanics **50** (2013) 141-151.

[51] P. A. Longwell, Mechanics of fluid flow, McGraw-Hill (1966).

[52] H. Lamb, Hydrodynamics, 6-th Edition, Cambridge University Press (1932).

[53] H. P. G. Darcy, *Les Fontaines Publiques de la Ville de Dijon, Exposition et Application des Principes à Suivre et des Formules à Employer dans les Questions de Distribution d'eau*, Paris, Victor Dalmont, 1856.

[54] S. P. Neuman, Theoretical Derivation of Darcy's Law, Acta Mech., **25** (1977) 153.

[55] S. Whitaker, Flow in Porous Media I: A Theoretical Derivation of Darcy's law, Transport in Porous Media, **1** (1986) 3-25.

[56] S. Whitaker, The Forchheimer Equation: A Theoretical Development, Transport in Porous media, **25** (1996) 27-61.

[57] H. Kim, T. Funada, D. D. Joseph, G. M. Homsy, Viscous Potential Flow Analysis of Radial Fingering in a Hele-Shaw Cell, Phys. Fluids **21** (2009) 074106.

[58] H. Gadêlha, J. A. Miranda, Effect of Normal Viscous Stresses on Radial Viscous Fingering, Phys. Rev. E **79** (2009) 066312.

[59] E. O. Dias, J. A. Miranda, Wavelength selection in Hele-Shaw flows: A maximum-amplitude criterion, Phys. Rev. E **88** (2013) 013016.

[60] L. D. Landau, E. M. Lifshitz, Course of Theoretical Mechanics Vol. 6: Fluid mechanics, Pergamon Press, 1959.

[61] H. Tani, Weakly nonlinear analysis on radially growing interface with the effect of viscous normal stress, J. Mol. Liquids, via online, DOI: 10.1016/j.molliq.2014.02.015.

[62] E. Alvarez-Lacalle, J. Ortin, J. Casademunt, Low Viscosity Contrast Fingering in a Rotating Hele-Shaw Cell, Phys. Fluids **16** (2004) 908-924.

[63] L. M. Martyushev, A. I. Birzina, Specific Features of the Loss of Stability during Radial Displacement of Fluid in the Hele-Shaw Cell, J. Phys.: Condens. Matter **20** (2008) 045201.

[64] H. Tani, A. Tani, Effect of the Wetting Layer on the Fingering Pattern in a Hele-Shaw Cell, J. Phys. Soc. Jpn. **83** (2014) 034401.